PNNL-29200

Nadir Pressure Exposure Estimates for the Existing Turbines at McNary Dam

September 2019

JA Serkowski
MC Richmond
CL Rakowski

U.S. DEPARTMENT OF ENERGY

Prepared for the U.S. Army Corps of Engineers
under a Government Order with the U.S. Department of Energy
Contract DE AC05 76RL01830

PACIFIC NORTHWEST NATIONAL LABORATORY
operated by
BATTELLE
for the
UNITED STATES DEPARTMENT OF ENERGY
under Contract DE-AC05-76RL01830

Printed in the United States of America

Available to DOE and DOE contractors from the
Office of Scientific and Technical Information,
P.O. Box 62, Oak Ridge, TN 37831-0062;
ph: (865) 576-8401
fax: (865) 576-5728
email: reports@adonis.osti.gov

Available to the public from the National Technical Information Service
5301 Shawnee Rd., Alexandria, VA 22312
ph: (800) 553-NTIS (6847)
email: orders@ntis.gov <https://www.ntis.gov/about>
Online ordering: http://www.ntis.gov

PNNL-29200

Nadir Pressure Exposure Estimates for the Existing Turbines at McNary Dam

JA Serkowski
MC Richmond
CL Rakowski

September 2019

Prepared for the U.S. Army Corps of Engineers
under a Government Order with the U.S. Department of Energy
Contract DE-AC05-76RL01830

Pacific Northwest National Laboratory
Richland, Washington 99354

Summary

This report documents a numerical modeling study conducted to assess the pressure environment and relative biological performance of the existing turbine runner design at the U.S. Army Corps of Engineers (USACE) McNary Dam to establish a baseline for comparison to planned replacement runner designs. Computational fluid dynamics (CFD) models of the turbine unit constructed for this study were analyzed using a streamtrace-based technique called the Biological Performance Assessment (BioPA), which was developed at the Pacific Northwest National Laboratory (PNNL). Specific project objectives were as follows:

- Build the complete geometry and CFD model of the existing turbine that includes the intake (including the trash rack extended-length submersible bar screen [ESBS], vertical barrier screen [VBS]), distributor, and draft tube.
- Simulate the turbine hydraulic environment (pressure, velocity, and turbulence fields) by running the CFD models at prototype scale using a rotating reference frame and including all runner blades for specific operating points (gross head, wicket gate angle, blade tilt angle) provided by the USACE.
- Estimate the magnitude and frequency of nadir pressure exposure for the specified turbine operating conditions. In addition, the BioPA passage quality indices (PQIs) for nadir pressure were calculated.
- Characterize draft-tube conditions and compare the CFD to the physical model results in the draft tube such as bulk flow distribution between the two barrels and velocities measured under the runner.
- Compare the CFD results for simulations using prototype and physical-model (1:25) scale geometries.

Before any pressure analyses were performed, the CFD models were checked against estimated power and discharge values for each operating point. Table S.1 shows that the models reproduced the target values with acceptable differences between the CFD results and plant estimates. However, note that the draft tube barrel A fraction did not follow the expected trend of having the majority of the discharge pass through the barrel. That general trend has been observed in physical models and prior PNNL CFD simulations of other Kaplan turbine units. After additional examination, the draft tube flow distribution discrepancy was judged to not have an appreciable impact on the runner pressure distributions.

Table S.1. CFD model settings and performance.

Op Point	Screen	Gross Head (ft)	Gate (deg)	Blade (deg)	Discharge (cfs) Plant	Discharge (cfs) CFD	Barrel A Fraction	Power (hp) Plant	Power (hp) CFD
PEAK	no	76.0	33.4	21.3	9,840	9,443	52%	76,000	73,119
UP1	no	76.0	38.3	26.9	12,172	12,083	47%	92,900	92,976
AB1	no	76.0	43.2	31.1	14,500	14,489	47%	108,500	110,562
PROP	no	73.0	47.7	33.0	16,300	15,833	47%	115,200	114,232
UP1	yes	76.0	42.0	25.2	12,282	11,872	38%	90,900	89,637
AB1	yes	76.0	49.1	28.8	14,500	14,188	41%	105,250	104,870

The report also includes comparisons to intake and runner-zone velocity measurements from the 1:25 reduced-scale physical model at the USACE Engineer Research and Development Center (ERDC).

The hydraulic conditions to which passing fish might be exposed were characterized using the BioPA technique. In the BioPA method, streamtraces are used to sample a CFD model and determine the probability of exposure to certain hydraulic stressors that are known to have adverse effects on juvenile salmonids. Note that BioPA results are only used as an estimate of *relative* passage risk and should not be

construed to be an absolute indicator of fish mortality or survival. Two streamtrace populations were analyzed. The DIST population represented a complete, uniform sampling of the turbine runner region and provided a turbine-average baseline. Previously performed field measurements of fish entering the turbine indicated that they are, in fact, unevenly distributed in the water column—the majority of turbine-passing fish enter just below the ESBSs that are installed in each unit bay to divert juvenile fish to an alternate route for passing the dam. These vertically distributed fish were simulated using the VERT streamtrace population that was based on hydroacoustic observations of fish distribution.

The two streamtrace populations were used to evaluate the CFD turbine models for exposure to low pressures, which have been shown to cause barotrauma injury in fish passing through turbines. Metrics for comparing exposures were based on data sets consisting of the magnitudes and locations of the lowest pressure along each streamtrace. Calculated and compared metrics included the nadir pressure PQI, which combines the frequency of low-pressure exposures with probabilities of adverse effects from such exposures as observed from laboratory investigations of barotrauma. Other metrics were the 10th percentile nadir pressure value and the fraction of nadir pressures below 1 atm (Table S.2).

Table S.2. Summary of nadir pressure metrics for DIST population.

Op Point	Screen	Head (ft)	Discharge (kcfs)	Barrel A%	Power (hp)	Population	PQI_{NP}	$10\%ile_{NP}$ (psi)	%NP<1atm (%)
peak	no	76.0	9,443	52%	73,119	DIST	493	19.6	1%
upper 1%	no	76.0	12,083	47%	92,976	DIST	488	15.2	12%
above 1%	no	76.0	14,489	47%	110,562	DIST	464	10.2	38%
prop	no	73.0	15,833	47%	114,232	DIST	458	9.4	39%
upper 1%	yes	76.0	11,872	38%	89,637	DIST	486	15.2	13%
above 1%	yes	76.0	14,188	41%	104,870	DIST	467	10.2	37%

The results for the nadir-pressure metrics are plotted in Figure S.1.

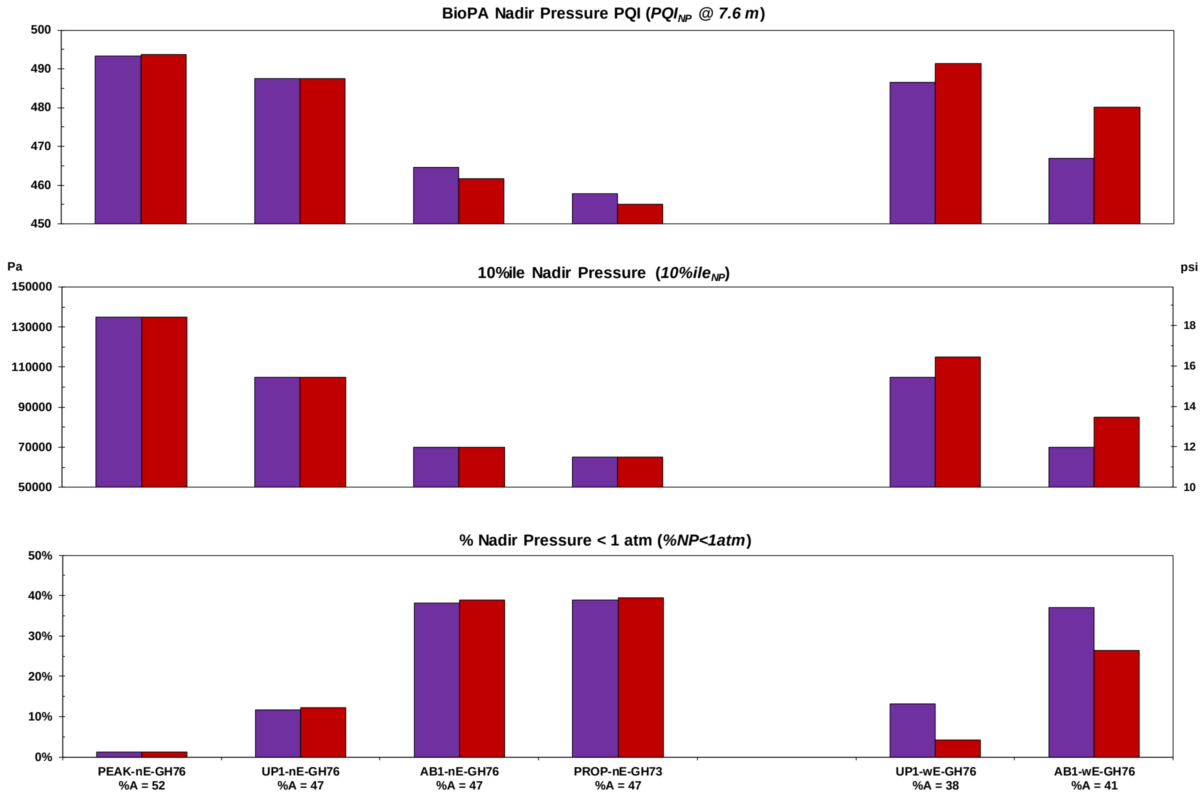

Figure S.1. Comparison of nadir pressure metrics for the DIST (purple) and VERT (red) populations.

Acknowledgments

The authors would like to thank a number of individuals who contributed to the successful completion of this project. At the U.S. Army Corps of Engineers, Walla Walla District, Jon Renholds and Martin Ahmann provided overall technical management and coordination of the project. Additionally, the reviews and discussions with Dan Patla (USACE HDC), and Bob Davidson (USACE ERDC) were valuable and greatly appreciated.

Acronyms and Abbreviations

atm	atmosphere
BioPA	biological performance assessment
CFD	computational fluid dynamics
cfs	cubic feet per second
cms	cubic meter(s) per second
DIST	Streamtrace seed location starting just upstream of the distributor (stay vanes)
DOE	The U.S. Department of Energy
ESBS	extended-length submersible bar screen
EPF	Laboratory for Hydraulic Machines of the Swiss Federal Institute of Technology
ERDC	Engineer Research and Development Center, USACE, Vicksburg, MS
ft	foot(feet)
hp	horse power
IHR	Ice Harbor Dam
in.	inch(es)
JDA	John Day Dam
kcfs	thousand cubic feet per second
kPA	kilopascal(s)
LDV	laser Doppler velocimeter
LEB	leading-edge blade
m	meter(s)
mm	millimeter(s)
MCN	McNary Dam
MRF	multiple reference frame
MW	megawatt(s)
NA	not applicable
Pa	pascal(s)
PNNL	Pacific Northwest National Laboratory
PQI	passage quality index
PRD	Priest Rapids Dam
psi	pounds per square inch
Rkm	river kilometer
RM	river mile
RMS	root mean square
RPM	rotation(s) per minute
s	second(s)
STS	submersible traveling screen

TKE	turbulence kinetic energy
URANS	unsteady Reynolds-averaged Navier-Stokes equations
USACE	U.S. Army Corps of Engineers
VAMCE	Voest Alpina MCE
VBS	vertical barrier screen (located in gate slot)
VERT	streamtrace seed location in the turbine intake
VERTnE	streamtrace seed location in the turbine intake – no ESBS
VERTwE	streamtrace seed location in the turbine intake – with ESBS

Contents

Figures

Tables

1.0 Introduction

This report documents a numerical modeling study to assess the biological performance of the existing turbine runner design at McNary Dam (MCN) to establish a baseline for comparison with planned replacement runners. Pacific Northwest National Laboratory (PNNL; operated by Battelle for the U.S. Department of Energy) performed this study for the U.S. Army Corps of Engineers (USACE), Walla Walla District.

1.1 Background

The USACE (or Corps) is in the process of developing new turbine runner designs to replace aging equipment (particularly aging runners in Units 1−14), improve hydraulic performance, and provide for a safer fish passage environment for the MCN powerhouse on the Columbia River. (This design process was previously used by the USACE at Ice Harbor Dam (IHR) on the Snake River and installation of the replacement runners is currently under way.

The purpose of the present study is to conduct a computational analysis of the existing Kaplan turbine runners at MCN to provide a baseline prior to the design of the new runners. The analysis will use the existing geometric design of the turbine to create a computational fluid dynamics (CFD) model of the turbine hydraulic environment. The model results will improve the understanding of the fish passage environment of the existing turbine, with a specific focus on the pressure distribution. The PNNL-developed Biological Performance Analysis (BioPA) software application was used to assess the potential exposure of fish to rapid decreases in pressure, which is a causative mechanism of mortality.

The research documented in this report is in support of USACE efforts to address the following 2008 Biological Opinion Reasonable and Prudent Alternatives (RPAs):

- RPA 21: “Configuration and Operational Plan for McNary Dam”
- RPA 54: “Monitor and Evaluate Effects of Configuration and Operation Actions”
- RPA 55: “Investigate Hydro Critical Uncertainties and Investigate New Technologies” including the development of new state-of-the-art turbines designed for improved fish passage.

1.2 Study Objectives

The overall goal of the project was to establish the baseline performance of the existing turbine runner design with respect to certain hydraulic stressors believed to be associated with fish injury. Specific tasks required to meet this primary objective were as follows:

- Build the complete geometry and CFD models of the existing turbines that include the intake (including the trash rack, extensible submersible bar screen [ESBS], and vertical barrier screen [VBS]), distributor, runner, and draft tube.
- Simulate the turbine hydraulic environment (pressure, velocity, and turbulence fields) by running the CFD models at prototype scale using a rotating reference frame and including all runner blades for six prescribed operating points (gross head, wicket gate angle, blade tilt angle) provided by USACE.
- Estimate the magnitude and frequency of nadir pressure exposure for the specified turbine operating conditions. In addition, the BioPA passage quality indices (PQIs) for nadir pressure were calculated.

Two subordinate objectives of the project were as follows:

- Compute metrics and develop visualizations to evaluate the potential utility of using CFD to evaluate flow through the draft tube.
- Assess the potential differences between flow conditions in prototype-scale and physical-model-scale simulations.

Note that due to unexpected results in the computed draft tube flow distributions (between the A and C barrels) were not completed.

1.3 Site Description

The McNary project is operated by the USACE Walla Walla District and is located along the southern border of Washington State on the Columbia River at Rkm 470 (RM 292) (Figure 1.1). The average annual river flow at the dam is approximately 4800 cubic meters per second (cms; 170,000 cubic feet per second [cfs]). The dam consists of a concrete powerhouse, navigation lock, two fish ladders, and a juvenile fish bypass facility. The construction of MCN began in 1947, and the 14 generators became operational in 1957. The powerhouse has an overall length of 433 m (1422 ft), and the 22-bay spillway is 400 m (1310 ft) long. An aerial view looking in a southerly direction is shown in Figure 1.2.

The powerhouse contains 14 identical Kaplan turbine units that were manufactured by S. Morgan Smith (now Voith Hydro). The runners have six blades having diameters of 7.12 m (280.5 in.) and rotating at 85.7 RPM. Each turbine is rated at 70 MW for a total plant rated capacity of 980 MW.

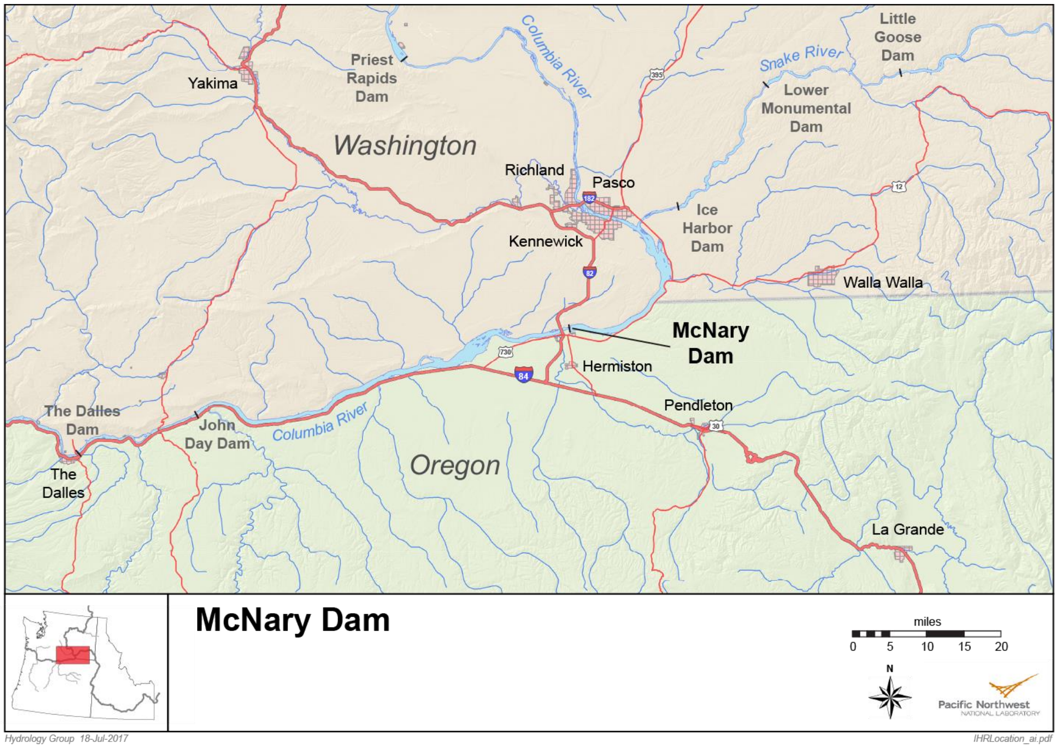

Figure 1.1. Location of McNary Dam on the Columbia River in southern Washington State.

Figure 1.2. McNary Dam on the Columbia River looking toward the northeast and showing (from top to bottom) the navigation lock, spillway, powerhouse, and fish bypass facility.

2.0 Test Conditions

The USACE provided PNNL with engineering drawings for the construction of the model geometry and a set of operating conditions for use in the present analysis.

2.1 Turbine Design

Existing Units 1–14 at MCN are of identical design and typical of those found at dams that have Kaplan turbines on the main stem of the Columbia and Snake Rivers. Each unit consists of a three-bay intake section fronted by a steel trash rack that feeds into a spiral case and distributor (Figure 2.1). The distributor uses 20 moveable wicket gates (Figure 2.2, left) to adjust and guide the flow into a vertical-axis Kaplan runner (Figure 2.2, right). The Kaplan design permits blade-angle adjustment for optimizing performance over a range of discharges and heads. The runner consists of six blades, has a diameter of 7.12 m (280.5 in.), and operates at 85.7 RPM. Flow exits the turbine through a double-barreled draft tube into the tailrace. Each unit is rated to 70 MW and typically operates with a gross head of about 22.9 m (75 ft) overflows ranging between (220 and 400 cms (8 and 14 kcfs). Intake bays may be equipped with ESBSs that extend from the ceiling and are designed to divert surface-oriented fish into a bypass channel. In addition, a VBS is a part of the fish diversion system in the intake.

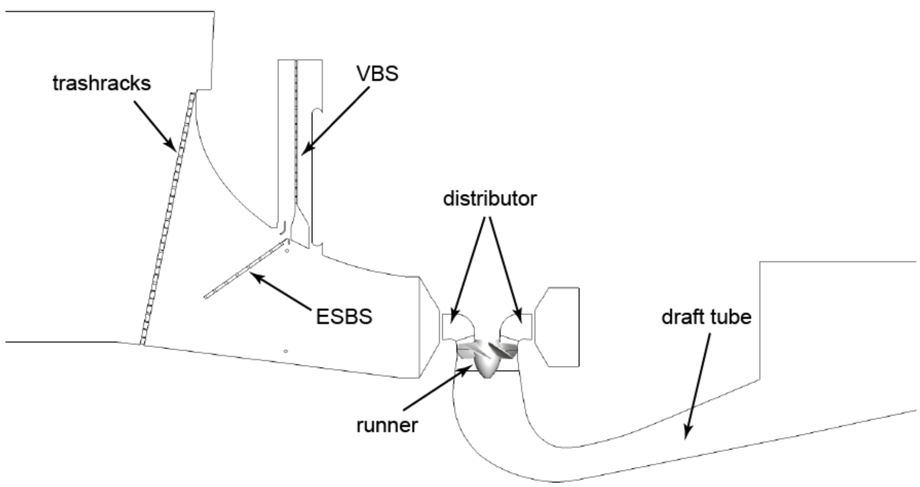

Figure 2.1. Turbine geometry features.

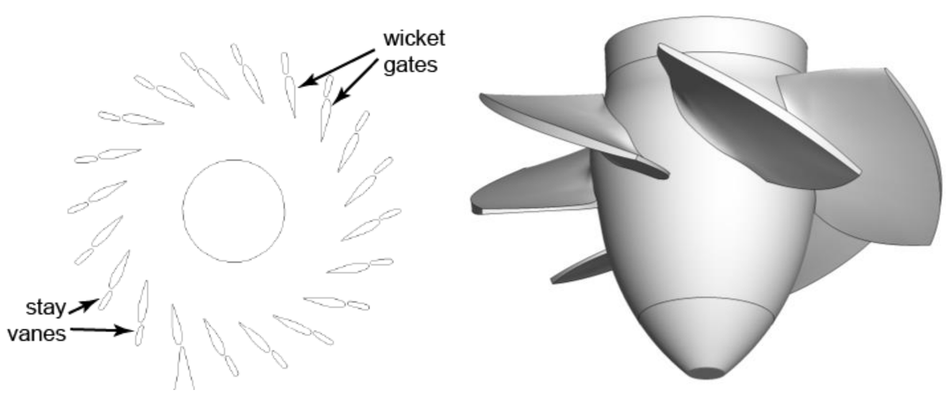

Figure 2.2. Stay vanes and wicket gates (plan view cut; left) and runner (right).

Late in the study, it was discovered that the runner cone (deflector) in the prototype ("actual") and the USACE Engineer Research and Development Center (ERDC) 1:25 scale physical model differed. The ERDC runner cone, created by the outside firm Voest Alpina MCE (VAMCE), had a larger tip diameter (Figure 2.3). After this discrepancy was discovered, ERDC replaced the cone in the physical model with the actual geometry. However, for comparisons with ERDC data sets in this report, model geometry was constructed with the "VAMCE" design, which was in place for the measurements at the time. In addition, the geometry created in this project was overlain on a photo of the actual runner (Figure 2.4) to further confirm that the actual cone corresponds to the installed version.

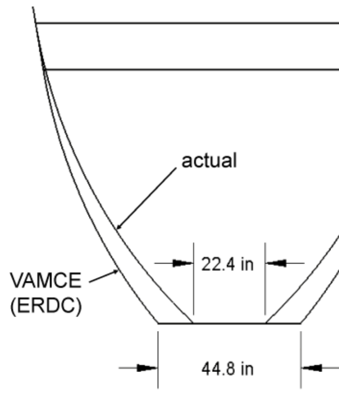

Figure 2.3. Difference between prototype ("actual") runner hub cone and that used by ERDC ("VAMCE").

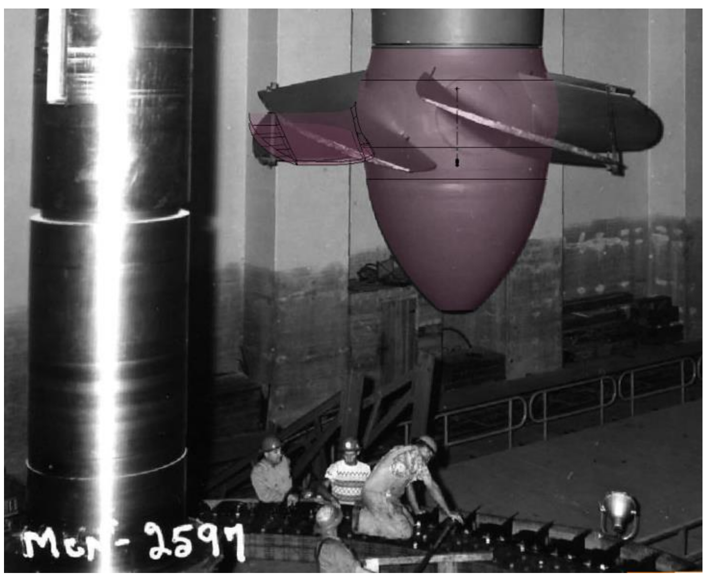

Figure 2.4. Overlay of turbine CAD geometry developed in this project with a photo of the actual MCN runner.

2.2 Operating Conditions

The operating points specified by the USACE for the prototype-scale CFD simulations in this study (Table 2.1) correspond to the conditions that represent the range of operating conditions for the existing runner at near a maximum head on the unit. This will allow comparison across the operating range with a head that is the worst case for nadir pressure conditions. It should be noted that these conditions do not necessarily fall within the expected fish-passage range for the existing runner but may for replacement runners. For example, the "above 1%" condition is beyond the fish-passage range—the "upper 1%" point being the top of that range. These conditions are subsequently referred to here as the "prescribed operations" to distinguish them from other conditions run to address different objectives in this study.

Additional operating conditions associated with data sets obtained by ERDC from their reduced-scale physical model are shown in Table 2.2. The table indicates the verification data set available from ERDC associated with each case.

Table 2.1. Prescribed operating conditions.

Model	Op Point	ESBS	Hub	Gross Head (ft)	Gate (deg)	Blade (deg)	Plant Estimates Discharge (cfs)	Plant Estimates Power (hp)
PEAK-nE-GH76	PEAK	No	actual	76.0	33.4	21.3	9,840	76,000
UP1-nE-GH76	UP1	No	actual	76.0	38.3	26.9	12,172	92,900
AB1-nE-GH76	AB1	No	actual	76.0	43.2	31.1	14,500	108,500
PROP-nE-GH73	PEAK	No	actual	73.0	47.7	33.0	16,300	115,200
UP1-wE-GH76	UP1	yes	actual	76.0	42.0	25.2	12,282	90,900
AB1-wE-GH76	AB1	yes	actual	76.0	49.1	28.8	14,500	105,250

Table 2.2. Operating conditions for verification runs (ERDC conditions).

Model	Op Point	ESBS	Hub	Gross Head (ft)	Gate (deg)	Blade (deg)	Meas. Discharge (cfs)	Est. Power (hp)	ERDC Velocities
ERDC-UP1-nE-GH73	UP1	no	VAMCE	73.0	37.8	25.7	12,560	89,300	draft
ERDC-14500-nE-GH73	MISC	no	VAMCE	73.0	42.2	29.9	14,620	-	intake/draft
ERDC-14500-wE-GH73	MISC	yes	VAMCE	73.0	48.8	28.2	14,620	-	intake/draft
ERDC-PROP-nE-GH73	PROP	no	VAMCE	73.0	47.7	33.0	16,537	115,200	draft
ERDC-PEAK-nE-GH76	PEAK	no	VAMCE	76.0	33.4	21.3	9,940	76,000	runner
ERDC-UP1-nE-GH76	UP1	no	VAMCE	76.0	38.3	26.9	12,525	92,900	runner
ERDC-UP1-wE-GH76	UP1	yes	VAMCE	76.0	42.0	25.2	12,525	90,900	runner

3.0 Methods

This section describes the tools and techniques used to generate the pressure comparison metrics presented in this report. The principal tools are CFD modeling and the BioPA software.

3.1 CFD Modeling

Modeling any hydro-turbine unit using CFD typically consists of three general steps: (1) preparing the model geometry and generating the mesh, (2) selecting the flow physics modeling options as part of the CFD setup, and (3) post-processing CFD results and validating them against plant and/or laboratory data (where available). The main outcome of the CFD modeling stage is to provide hydraulic conditions under which the BioPA runs are conducted in post-processing.

3.1.1 CFD Model Preparation

The model geometry was created in SolidWorks for each of the operating conditions in Table 2.1 and Table 2.2 based on a set of engineering drawings provided by the USACE. Therefore, 13 Parasolid files were generated and included the trash racks, intake with three bays, ESBSs, the VBSs, distributor, runner, and draft tube. An extended outflow section was added downstream of the draft tube to allow for exit flows to develop over longer distances, which facilitates convergence of the numerical solution. A view of the intake geometry is shown in Figure 2.1. The distributor and runner portions of the geometry are represented in full; that is, the models included all distributor vanes and runner blades.

The mesh generation and CFD modeling were completed using the commercial software STAR-CCM+ v12.06 (CD-adapco 2016). The mesh consisted of various regions (labeled as intake, trash racks, ESBS, VBS, distributor, runner, and draft) continuously connected through interfaces. While most of these interfaces represented a continuous transition across connected regions (e.g., intake/distributor), some were set as porous baffles to represent resistances from screens/plates. The mesh generation tools in the software include polyhedral cells, which allowed for different resolutions and cell distributions according to local requirements, typically driven by the expected flows. For instance, finer cells on the blade runner ensure a better representation of the large velocity gradients expected on that solid wall. The averaged dimensionless wall distance (y+) of the first cell of the blades was in the range $5 < y+ < 10$. The computational mesh sizes for the regions comprising the intake, distributor, runner, and draft tube varied, but were typically on the order of 15M, 8M, 7M, and 5M, respectively. The intake configurations with and without the screens were created and used across multiple operational scenarios so that only the distributor and moving region changed between runs. The flow results were checked to ensure that resultant y+ values for the meshes were acceptable throughout the flow domain.

3.1.2 Modeling Assumptions and Setup

The CFD software allows us to model the physics of the flow following modeling standards that are widely practiced in the turbine design industry. Such practices entail the selection of turbulence-modeling schemes to represent the highly dynamic flows at relatively long time steps, thereby allowing for a representation of mean flow conditions. The second-order convection scheme was selected within the segregated flow solver in transient mode, with the k-ω SST turbulence model in its unsteady Reynolds-averaged Navier-Stokes (URANS) version. The time solver accuracy was set as first-order with a constant time step of 0.1 second ($\Delta t = 0.1$ s). A flow-through time from the ESBS region to the draft tube exit is approximately 30 s. Based on this time reference, the flow conditions were simulated for a period of at least two flow-through times (60 s, but often longer for monitored parameters such as draft tube flow splits to stabilize) before an additional simulation time of 30 s, during which the velocity components, pressure, and turbulent kinetic energy were time-averaged. These averaged parameters were exported to be used for the BioPA calculations in post-processing.

Typically, boundary conditions at the model inlet and outlet were set so that the discharge through the unit was driven by a differential pressure (gross head) particular to each operating condition. A steady-state, multiple reference frame (MRF) approach was used to model the effects of the rotating motion of the runner without the use of a computationally expensive unsteady moving-mesh simulation. The rotation rate was set equal to 85.7 RPM, except for the discharge ring and the headcovers, which were set to being stationary. The nominal water surface at the forebay and the tailrace were represented as slip walls. The full unit model consists of multiple volume regions connected at interfaces. These interfaces connect regions directly when they represent a continuous medium or were set as porous baffles when resistance was represented (e.g., screens, perforated plates, etc.). Only the interface between the moving region and the draft tube was set as an indirect mixing-plane, as is typically done in similar turbo-machinery applications, where the non-uniform velocity field in the rotating region is circumferentially averaged at the interface and then passed as the inflow to the draft tube (CD-adapco 2016).

The trash rack in the model geometry included the main vertical and horizontal structural components supporting the small vertical racks, which were modeled as a porous baffle interface with a porosity of 92% and a resistance coefficient of 0.17. The porosity was obtained from the geometric construction of the racks (thickness and spacing). The resistance coefficient was based on the experimental work of Ghamry and Katopodis (2012), in which one tested configuration (referred to as Test 1) was considerably similar to the geometry of the McNary trash racks.

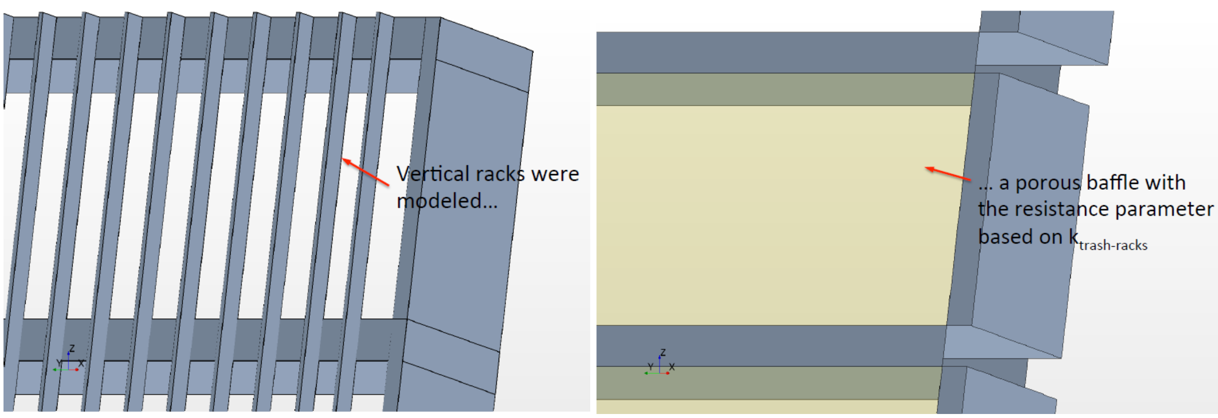

Figure 3.1. The vertical racks (left) were modeled as a porous baffle with resistance parameters calculated from the geometric construction and a resistance coefficient based on Test 1 of Ghamry and Katopodis (2012).

The ESBS was represented as an assembly composed of two porous baffles: a meshed screen and a perforated plate. The mesh screens and perforated plate installed in the ESBSs were tested at the USACE-ERDC as part of an extensive hydraulic model investigation of numerous configurations of extended submerged bar screens (Davidson 2004). According to the USACE-Walla Walla District (personal communication), the ESBS currently in place at the McNary Dam is configured as a Hendricks bar screen with 0.125" spacing mounted on a frame, as well as a perforated plate (Plate B in Figure 3.2). The report by Davidson (2014) provides details of the loss coefficient determination for these resistances in the form of:

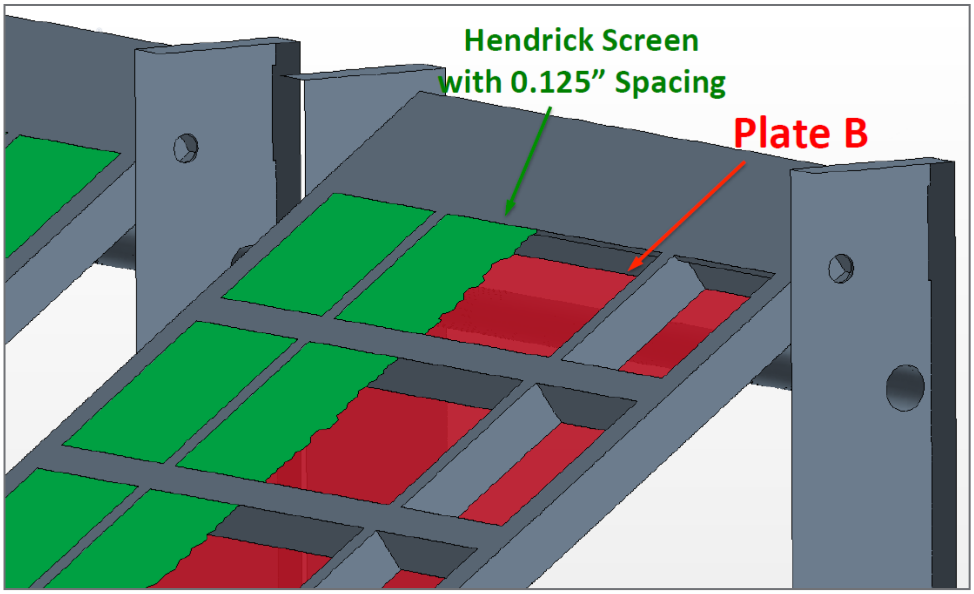

Figure 3.2. Representation of the ESBS assembly in the CFD model.

- Approach Velocity vs. Head Loss (Figure 3.3)
- Normalized Approached velocity vs. Head Loss (to obtain the slope representing the resistance coefficient K)
- The porosity (ϕ) and resistance coefficient (K) in tabulated form.

The tabulated values were used to determine the pressure loss (ΔP) through the interface, which, in the CFD flow simulation, is modeled with porosity (ϕ) and inertial coefficients (α), using Equation (3.1) :

$$\Delta P = -\rho(\alpha|V_n| + \beta) \cdot V_n \tag{3.1}$$

The viscous resistance coefficient (β) was assumed to be zero. For the VBSs, we followed the guidelines provided by the USACE Portland office and were used in similar simulations of a VBS. Table 3.1 lists the parameters used in the present simulations.

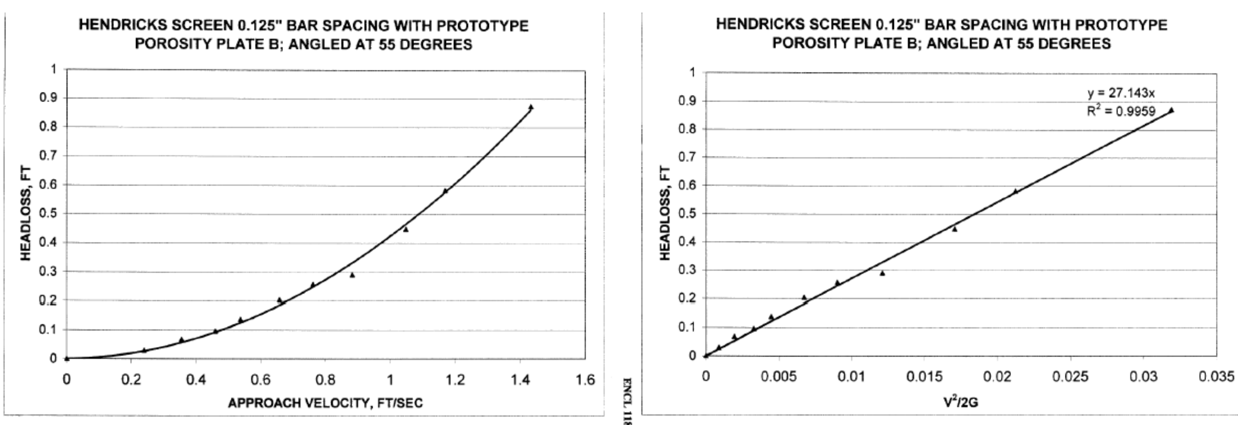

Figure 3.3. The head loss as a function of the approach velocity in the test flume, when the resistance configuration had a perforated plate and a Hendricks screen like that currently installed in the ESBS at the McNary units.

The VBS (see Figure 2.1) was modeled as a porous baffle with prescribed porosity and resistance. The remaining solid boundaries were set as no-slip walls.

Table 3.1. Porous baffle parameter values.

	Porosity (ϕ)	Inertial resistance (α)
Trash racks	92.0 %	0.085
Perforated plate	25.0 %	11.81
Screen	58.0 %	2.22
Vertical barrier screen	20.0 %	30.3

3.1.3 Post-Processing and Comparison to Measured Velocities

The following quantities were monitored during the transient flow simulation: shaft power, discharge, wall y+ on the blade surface, and flow splits at each intake bay and draft tube barrel.

The BioPA calculations were based upon the time-averaged fields for velocity, pressure, specific dissipation, and turbulent kinetic energy computed from the CFD simulations. These fields were exported into a Tecplot format file (PLT) for all regions in the model. Mean-velocity gradients were exported to calculate statistics related to hydraulic shear (i.e., the strain-rate tensor magnitude).

Velocity measurements for two cases listed in Table 2.2 (ERDC-14500-nE-GH73 and ERDC-14500-wE-GH73) were collected using laser Doppler velocimetry (LDV) in a 1:25 reduced-scale physical model of the MCN turbine, intake, and draft tube, located at the USACE ERDC. Figure 3.4 shows the measurement locations for both operating points (“No ESBS” configuration on the left; “with ESBS” on the right). Measurements were obtained at two transects (near the trash racks and past the ESBS) at both operating points but only in one intake bay for the case AB1-nE (Bay A, the one typically with the largest discharge). There are four vertical lines per bay and location.

Data for mean velocities were recorded for both the stream-wise and vertical directions (U and W velocities, respectively). Corresponding CFD results were compared against the values from the downstream transect (ESBS) as a means of validating the quality of the simulated results. For this purpose, the three-dimensional (3D) flow solution of velocity was interpolated at the corresponding measurement locations.

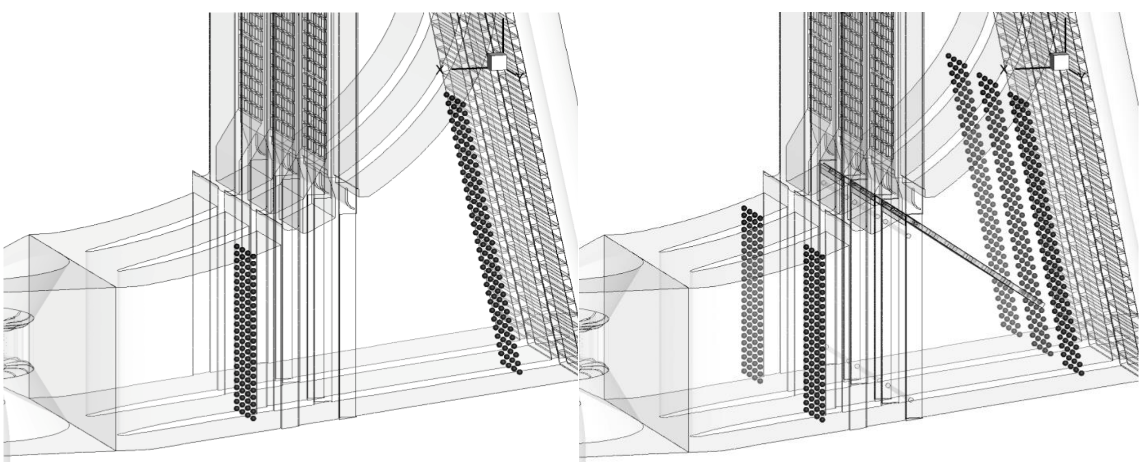

Figure 3.4. Locations of LDV measurements for the operating points labeled as ERDC-14500-nE-GH73 (left) and ERDC-14500-wE-GH73 (right) in Table 2.2.

3.2 BioPA

The BioPA method uses a CFD model to simulate the hydraulic environment of a potential passage route to estimate the probability of exposure to certain stressors believed to adversely affect the survival of fish. The BioPA consists of four components: the CFD model that describes the hydraulic environment (see Section 3.1), a streamtrace-based scheme for proportionately sampling the model domain, calculation of exposure probabilities, and conversion of these exposures to a PQI using biological dose-response data.

After the CFD model results are generated, the BioPA samples them using a set of streamtraces. Streamtraces are the paths followed by neutrally buoyant, massless particles through the simulated velocity field. The BioPA tool uses the values of hydraulic variables sampled along these streamtraces to estimate exposure during turbine passage. The streamtraces originate at seed locations that are placed upstream of the runner, where adverse pressure conditions are expected. Each seed location may be weighted to simulate an assumed initial fish distribution. The combination of seed locations and weightings defines the sample population. To simulate a full-turbine fish population, the seeding pattern might be uniformly distributed over the entire intake entrance to capture the complete set of possible entry points the fish use to enter the unit. If the distributions of fish in the intake are known from field measurements (e.g., using hydroacoustics instrumentation), seed arrays can be designed to more realistically capture likely passage routes through the turbine.

One important characteristic of the turbine CFD model used in this version of the BioPA is that the runner blades are in a fixed location, although their motion is modeled with an MRF. Consequently, a streamtrace released from a certain point will always encounter the runner at the same blade position. If the runner were actually rotating, a streamtrace released at a random time would encounter the blade at some random position in its rotation, which would differ depending on the time of release. Because the location of a passage route with respect to the runner blade can make a significant difference in its hydraulic exposure, the BioPA must account for this time-dependent phenomenon.

The BioPA addresses time-dependence at the runner using a path-splitting scheme. In this scheme, as a streamtrace enters the MRF region of the CFD model, it is split into several new streamtraces to sample the runner at different positions. To accomplish this, the starting points of the new streamtraces are offset at uniform angular increments around the runner axis (Figure 3.5). The effect is to capture the streamtrace passages at a set of alternate, uniformly spaced blade positions. After passing the MRF region, the paths are interrupted again and the ends of the paths are rotated back around the runner axis. Sensitivity analysis has indicated that splitting streamtraces into 10 paths (separated by 6.0° for a six-bladed runner) is adequate for capturing the range of possible hydraulic conditions associated with all possible blade positions. A streamtrace from a particular seed in the intake will then take a single path until it reaches the first interface upstream of the runner, whereupon it will split into 10 separate paths for the remainder of its passage through the turbine.

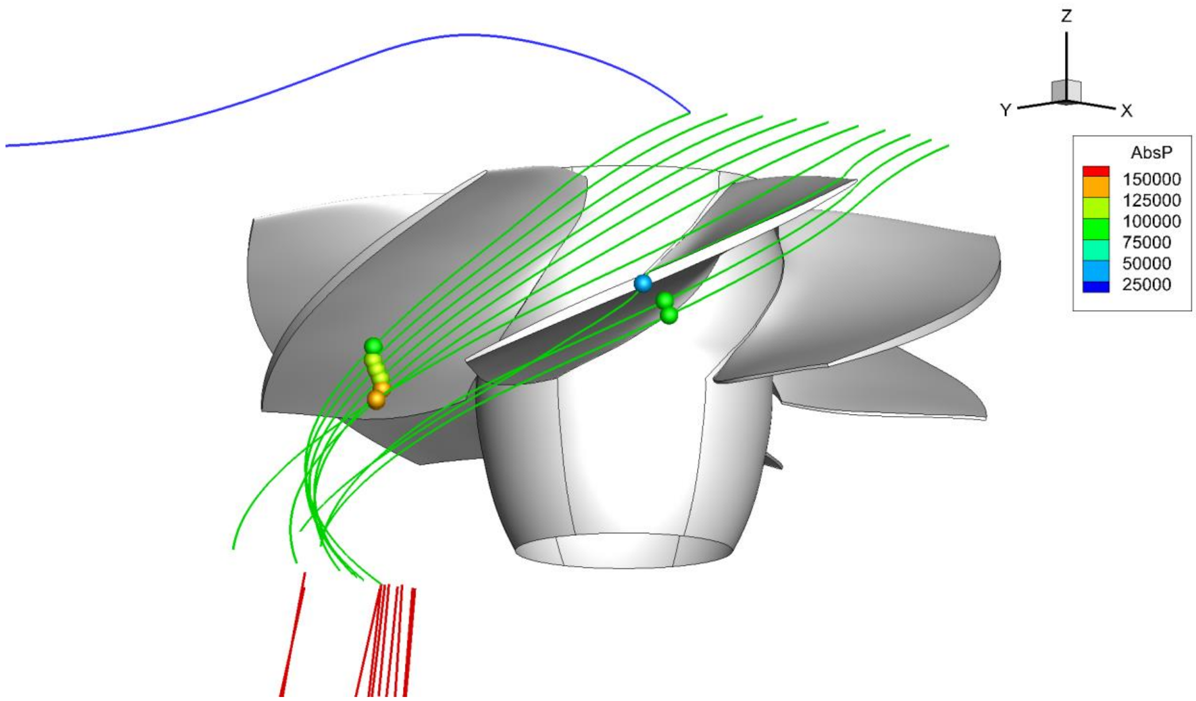

Figure 3.5. BioPA path-splitting scheme: the streamtrace from intake (blue) is split into 10 uniformly rotated streamtraces (green) to sample the runner at various "positions"; streamtraces are rotated back after passing through the runner (red).

Each streamtrace sample consists of a record of simulated hydraulic variable values along closely spaced points on the path. Data include the coordinates of each point, flow velocity and velocity gradient, absolute static pressure, and turbulence kinetic energy (TKE). Using these variables, the BioPA application calculates the following stressor statistics that have known correlations with adverse effects on fish: nadir pressure, maximum shear, maximum turbulence, and leading-edge blade (LEB) strike probability and intensity. The nadir pressure is the minimum pressure along the streamtrace, which usually occurs under the runner blade on the suction side or at the blade tip. Maximum shear along each path is computed from the magnitude of strain rate, which is a function of the velocity gradients of the model flow field. Maximum turbulence is the highest value of TKE encountered along the stream path. The LEB strike probability assessment was not within the scope of the present study.

After stressor values are determined for each streamtrace, a histogram for each stressor is used to develop a discrete exposure probability distribution (Figure 3.6). This probability distribution represents the hydraulic exposure for the given seed array. The exposure estimate may be adjusted by weighting each streamtrace according to the probability a fish enters the turbine at that corresponding seed location. For example, if fish tend to be surface oriented, higher weights would be assigned to exposures from streamtraces originating closer to the top of the intake.

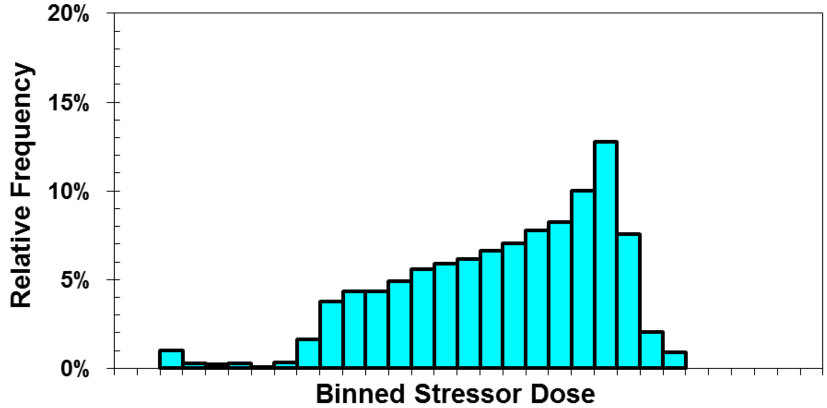

Figure 3.6. Sample exposure distribution.

The final component of the BioPA is the determination of the biological response to the computed hydraulic stressors and the estimation of the relative passage risk. Laboratory studies designed to measure the response of fish to various conditions (Neitzel et al. 2000; Odeh et al. 2002; Neitzel et al. 2004; Amaral et al. 2007; Brown et al. 2012) were used to construct dose-response relationships for each BioPA stressor (Figure 3.7). The adverse responses observed in these studies ranged widely in type and severity: from grave injuries resulting in immediate death to temporary impairments that might increase the risk of predation. Moreover, the number and species of test subjects varied and the methods of identifying responses were not consistent. The nadir-pressure studies were the most comprehensive and resulted in a sigmoid-shaped dose-response curve, while the turbulence study was the least definitive and produced only a single threshold value where an adverse response began to be observed. Consequently, the probability of adverse response, in the context of the BioPA, is used as an estimate of *relative* passage risk and must not be construed to be an indicator of absolute fish mortality or survival.

The metric generated by the BioPA is called the PQI (passage quality index). The PQI for a particular stressor is based on the product of the exposure probability to a stressor dose and the adverse-response probability resulting from this dose. It is computed as follows:

$$PQI_S = int\left(500 * \sum_{i=1}^{i=n} P_e(S_i) \cdot P_{ar}(S_i)\right) \tag{3.3}$$

where $P_e(S_i)$ is the probability of exposure to a particular level of stress, S_i, and $P_{ar}(S_i)$ is the probability of an adverse response from that same level of stress. The summation is performed over all of the n bins in the exposure histogram and multiplied by 500 to yield an integral index value between 0 and 500. This formulation yields higher numbers for more favorable passage conditions and lower numbers for less favorable ones.

As with any predictive method, the BioPA process relies on confidence in certain data sets and assumptions about how they may be used. Some of the assumptions and limitations, which are detailed by Richmond et al. (2014), are as follows:

- Streamtraces do not represent fish paths, but, rather a method of statistically sampling the turbine environment.
- It is difficult to validate CFD models in the absence of detailed measurements at the prototype.
- The laboratory dose-response studies of fish exposed to hydraulic conditions are a small number and the studies are of limited scope (fish species, life stage).

- Fish characteristics, such as acclimation depth for in-river migrants, are uncertain and affect the PQI estimates.

3.3 Pressure Characterization

A primary objective of the study presented here was to compare the pressure characteristics of the various turbine operations because laboratory studies (Brown et al. 2012) indicate that low pressures pose a risk to juvenile salmonids. BioPA streamtraces were used to sample pressure throughout the turbine and several metrics were generated for comparison purposes. Two seeding configurations were developed to provide information about different potential fish populations.

3.3.1 Seeding Configurations and Populations

The BioPA can simulate passage conditions for specific distributions of fish entering the turbine. These distributions are referred to here as fish populations. Fish populations are simulated by the arrangement and weighting of BioPA streamtrace seeds. Two fish populations were considered in this study: uniform and vertically distributed. The uniform population (called DIST in this study because seeds were located at the entrance to the distributor) was generated using a seeding array consisting of 3204 uniformly distributed points, spaced 0.2 m apart (Figure 3.8). While this distribution is not likely to occur in the prototype, it provides a thorough sampling of the entire runner environment, even supplying information about regions that are unlikely to ever be visited by fish. As such, it serves as a baseline for comparison with the other simulated populations.

The vertically distributed populations (VERTnE and VERTwE) were designed to simulate the vertical distribution of fish in the intake based on hydroacoustic measurements by Ham et al. (2013). Ham et al. (2013) measured distributions both upstream (“guided”) and downstream (“unguided”) of the ESBS in all three units of four turbine bays at two operating levels (peak and upper 1%). For this study, the unguided measurements were used to develop a distribution for the cases without a deployed ESBS (Figure 3.9) and the guided for those cases with an ESBS (Figure 3.10). To model these cases, a uniform distribution of 6570 seeds, spaced 0.2 m apart, was constructed on the vertical plane coinciding with the downstream slides of the ESBS slots. A BioPA was run for all seeds, but computed exposures were then weighted by the guided distribution to produce the VERTnE population and the unguided distribution to produce the VERTwE population.

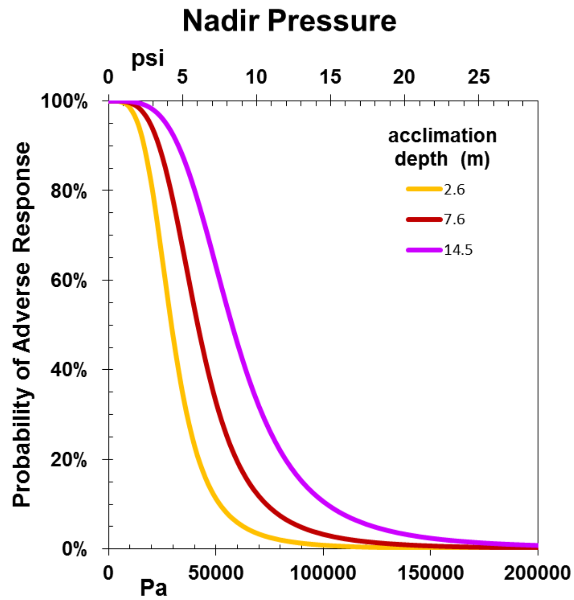

Figure 3.7. Nadir pressure dose-response relationships used by the BioPA tool. Note that PQI calculations in this report assumed an acclimation depth of 7.6 m.

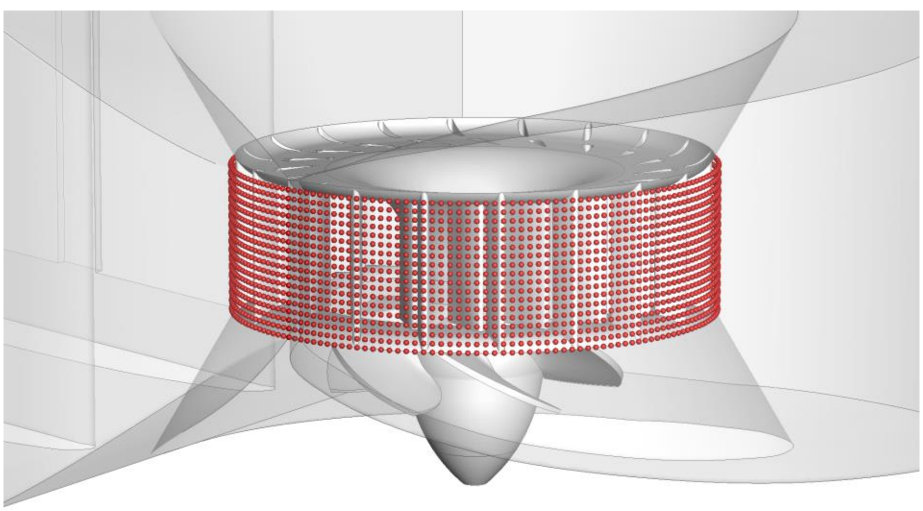

Figure 3.8. Distributor (DIST) seed distribution.

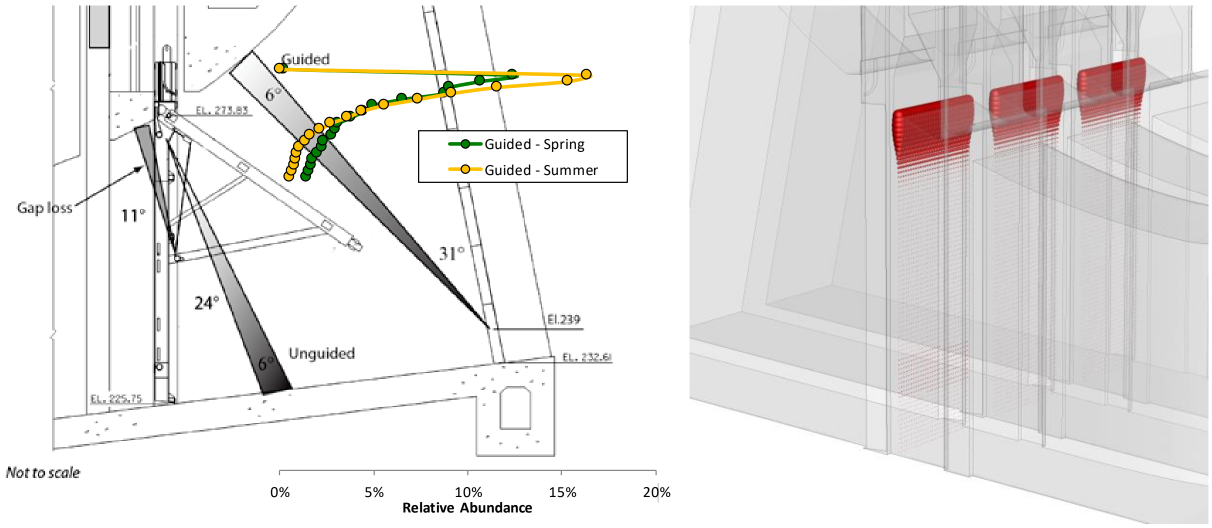

Figure 3.9. Vertical (VERTnE) fish distributions for cases with no ESBS based on measurements by Ham et al. (2013) with points sized by relative fish abundance.

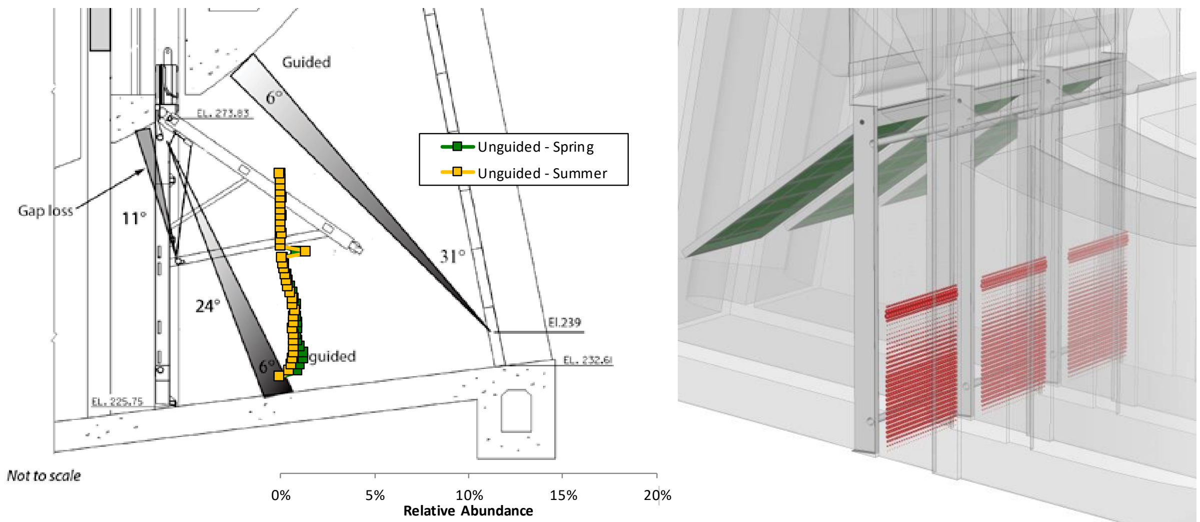

Figure 3.10. Vertical (VERTwE) fish distributions for cases with an ESBS based on measurements by Ham et al. (2013) with points sized by relative fish abundance.

3.3.2 Pressure Metrics

Three metrics were used to compare pressure characteristics among the designs and operations. All are based on the lowest detected pressure (nadir pressure) observed on a BioPA streamtrace. The nadir pressure, along with fish acclimation pressure, are the key factors in determining barotrauma for fish passing through turbines (Brown et al. 2012). The primary metric is the BioPA nadir pressure PQI (PQI_{NP}) described in Section 3.2, which combines the frequency of exposure to low pressures with an estimate of its relative potential to adversely affect a fish. A higher PQI_{NP} indicates a safer passage condition.

Calculation of PQI_{NP} requires an assumed fish acclimation depth. As fish travel deeper in the water column, pressure compresses their bodies, reducing their volume and their buoyancy. To maintain neutral buoyancy, salmonids adjust the pressure in their swim bladders. Deeper acclimation requires higher swim-bladder pressure, resulting in greater susceptibility to barotrauma for a given nadir-pressure exposure. Fish acclimation is very difficult to measure in the field. Moreover, physostomes, which include salmonids, may have the ability to rapidly depressurize by "burping" excess air from their swim bladders (Brown et al. 2012). This action, if taken, would tend to reduce their vulnerability to barotrauma. Pflugrath et al. (2012) used laboratory experiments to determine an upper bound on acclimation depth of about 11 m (median 6.7 m). Deng et al. (2014), tracked swimming depths of fish prior to turbine entry based on the assumption that they were acclimated and observed a median depth of 7.6 m in the IHR forebay. For the purpose of this study, all fish were assumed to have an acclimation depth of 7.6 m.

In addition to PQI_{NP}, two other pressure metrics were computed for this study: 10th-percentile nadir pressure ($10\%ile_{NP}$) and percent nadir pressures below 1 atm *(%NP<1atm*). Neither of these metrics involves explicit adverse-effect responses or assumptions of acclimation depth; rather, they each reflect the qualitative finding that exposure to low pressures can harm fish. The $10\%ile_{NP}$ statistic represents the pressure below which the lowest 10% of exposures occur. For example, a $10\%ile_{NP}$ of 7 psi would indicate that 10% of the population would experience at least one instance of pressures below 7 psi. Lower values would suggest more harmful conditions.

The *%NP<1atm* statistic relates nadir pressure exposure to atmospheric pressure by determining the fraction of the population that is exposed to nadir pressures below 1 atm (101325 Pa or 14.7 psi). This statistic uses a somewhat less arbitrary reference point than that used by the $10\%ile_{NP}$ statistic. The relevance of 1 atm is that this pressure is associated with the shallowest probable acclimation depth in passing fish. That is, fish acclimated to any depth below the surface will have internal pressures higher than 1 atm. Therefore, this statistic indicates the *minimum* possible fraction of the population that experiences a nadir pressure lower than its acclimation pressure. Note that, unlike the PQI_{NP} and $10\%ile_{NP}$ metrics, higher values of *%NP<1atm* may indicate *more harmful* conditions.

3.4 Scaling Effects

The reduced-scale physical model of the MCN turbine at ERDC was built at a 1:25 scale. BioPA uses prototype-scale geometry because hydraulic exposure must be known at full scale for use with available dose-response relationships. Results from the ERDC Froude-scaled physical models can be up-scaled to prototype values using the relationships shown in Table 3.2. To analyze the effects of reduced-scale modeling in the context of BioPA, CFD modeling results at prototype scale and physical-model scale were compared.

The operating points selected for this analysis included one of the prototype-scale conditions, UP1-nE-GH73, and several ERDC cases associated with intake and under-runner velocity measurements listed in Table 2.2. New computer models were run at a 1:25 reduced and designated with a "-1to25" suffix in the nomenclature. Note that all CFD models used for the evaluation of scaling effects used the VAMCE runner cone (see Section 2.1) to be compatible with available ERDC data sets.

Reduced-scale model results were up-scaled using formulas (Table 3.2) applied in Tecplot to create results files at the prototype scale. BioPA analyses were performed on the up-scaled files and the results were compared to those from the corresponding models run at prototype scale. Comparison metrics included PQIs, the additional pressure metrics described in Section 3.3.2, and various visualizations.

Table 3.2. Froude scaling relationships for 1:25 models.

Variable	Units	Relationship	Factor[(a)]
Scale	-	25	25
Length	L	S	25
Time	T	$S^{0.5}$	5
Runner Rotation	1/T	$1/S^{0.5}$	0.2
Velocity	L/T	$S^{0.5}$	5
Velocity Gradient	(L/T)/L	$1/S^{0.5}$	0.2
Pressure	$M/(L*T^2)$	S	25
TKE	L^2/T^2	S	25
Power	$(M*L^2)/T^3$	$S^{3.5}$	78125
Discharge	L^3/T	$S^{2.5}$	3125
Gross Head	L	S	25

(a) The factor is the number by which the reduced-scale model variable is multiplied to obtain the prototype-scale value.

3.5 Draft Tube Analysis

Minimizing turbulence on the draft tube and balancing the flow through the two barrels is an important factor for turbine efficiency and reducing fish passage impacts. ERDC made LDV measurements at the draft-tube and under-runner locations shown in Figure 3.11 for the conditions specified in Table 2.2. These measurements can provide information about the flow at those points. The under-runner measurements were designed to evaluate the flow swirl entering the draft tube and the draft-tube data provided information about flow balance. Flow splits were calculated from the LDV data by integrating the downstream velocity components over the cross-sectional area to compute discharge through each barrel.

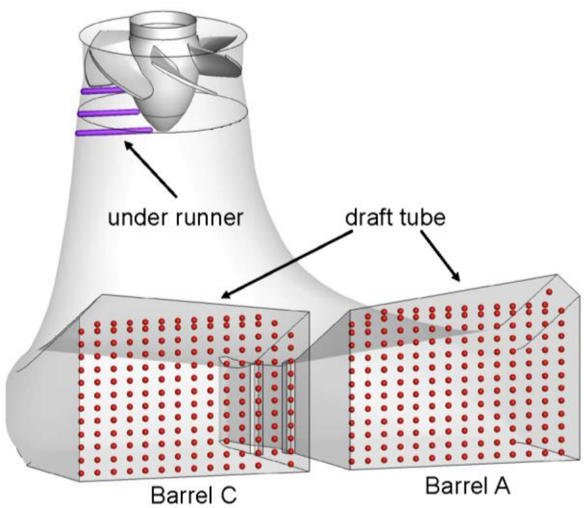

Figure 3.11. Locations of LDV measurement made by ERDC.

The ERDC data were compared to CFD models to bolster confidence in the draft-tube characterization of the prototype-scale operations models. Note that all CFD models used for comparing to ERDC data used the VAMCE runner cone (see Section 2.1).

4.0 Results and Discussion

Before any pressure analyses were performed, the CFD models were checked to verify that they produced acceptable comparisons to estimated power and discharge values. Available velocity data collected by ERDC were also compared. After the satisfactory agreement with target values was achieved for all models, BioPA software analyses were performed on each model using the intake seed populations DIST (distributor), VERTnE (no ESBS), and VERTwE (with ESBS). Metrics were then computed for each model and population combination to produce estimates and analyses of full-turbine passage conditions. Finally, analyses were performed to evaluate the effects of model scaling and characterization of draft-tube flow conditions.

4.1 CFD Model Verification

Modeling of flow through turbines using CFD has been used successfully by industry and researchers for many years. The techniques are well established and enjoy widespread credibility. Nevertheless, it is always essential to verify each modeling activity as thoroughly as possible against all available data. The difficulty in collecting relevant measurements from the prototype and the limited availability of physical-model data make this task challenging. For this study, verification data sets included plant estimates of power and discharge at the prototype─referred to here as hydraulic performance─and measured velocities using LDV data sets from the 1:25 physical model at ERDC.

4.1.1 Hydraulic Performance

The plant estimates for the prototype operating points listed in Table 2.1 and the discharges measured by ERDC listed in Table 4.1 were compared to CFD models. Plant estimates were obtained from USACE and are usually based on performance studies conducted at a turbine test stand model and/or the prototype at a specified number of conditions. The limitations of these estimates include the difficulty of accurately measuring discharge in the field and the validity of interpolating the performance data to conditions not explicitly tested. For the ERDC models, the discharge could be accurately measured, but power data were not available.

Table 4.1 summarizes the hydraulic performance comparisons. The cases are grouped by the presence of the ESBS and then ordered by discharge. The CFD models generally slightly underestimated both power and discharge. The relative differences (%Δ) do not appear to be proportional to the target values of discharge or power. The underestimation may result from greater hydraulic losses associated with the turbulence model implemented in the CFD simulations. Although the k-ω SST turbulence model is a standard choice for turbulent flows in the turbomachinery industry, it may amplify turbulence-related losses in the draft tube and other areas with strong flow recirculation. While all turbulence models for CFD have strengths and weaknesses, a particular weakness of the k-ω model is that it can induce flow separation prematurely. In general, the level of agreement between modeled, plant estimates, and laboratory data increased our confidence in the accuracy of this CFD modeling work.

Table 4.1. Hydraulic performance comparisons between plant estimates and prototype-scale CFD models.

	Discharge (cfs)				Power (hp)			
Model	Target	CFD	Δ	%Δ	Target	CFD	Δ	%Δ
PEAK-nE-GH76	9,840	9,443	-397	-4%	76,000	73,119	-2,881	-4%
ERDC-PEAK-nE-GH76	9,940	9,478	-462	-5%	76,000	71,765	-4,235	-6%
UP1-nE-GH76	12,172	12,083	-89	-1%	92,900	92,976	76	0%
ERDC-UP1-nE-GH76	12,525	12,076	-449	-4%	92,900	92,917	17	0%
ERDC-UP1-nE-GH73	12,560	11,431	-1,129	-9%	89,300	84,280	-5,020	-6%
AB1-nE-GH76	14,500	14,489	-11	0%	108,500	110,562	2,062	2%
ERDC-14500-nE-GH73	14,620	13,717	-903	-6%	-	100,072	-	-
PROP-nE-GH73	16,300	15,833	-467	-3%	115,200	114,232	-968	-1%
ERDC-PROP-nE-GH73	16,537	15,861	-676	-4%	115,200	115,382	182	0%
UP1-wE-GH76	12,282	11,872	-410	-3%	90,900	89,637	-1,263	-1%
ERDC-UP1-wE-GH76	12,525	11,880	-645	-5%	90,900	89,500	-1,400	-2%
AB1-wE-GH76	14,500	14,188	-312	-2%	105,250	104,870	-381	0%
ERDC-14500-wE-GH73	14,620	13,725	-895	-6%	-	97,924	-	-

4.1.2 Velocity Comparisons

The CFD results were compared against LDV velocity measurements collected from the ERDC 1:25 scale physical model (these models had the VAMCE cone installed). Figure 4.1 shows direct comparisons between the two data sources, with the data points colored by location. The narrow range of values in the absence of the ESBS was an indicator of a tendency for flow conditions to develop more uniformly within the intake at the AB1-nE operating point than at the AB1-wE one. Because the majority of data points lie near the bisecting line, we considered that the agreement between the two data sources was satisfactory, with potential improvements to be made in modeling flows near the walls.

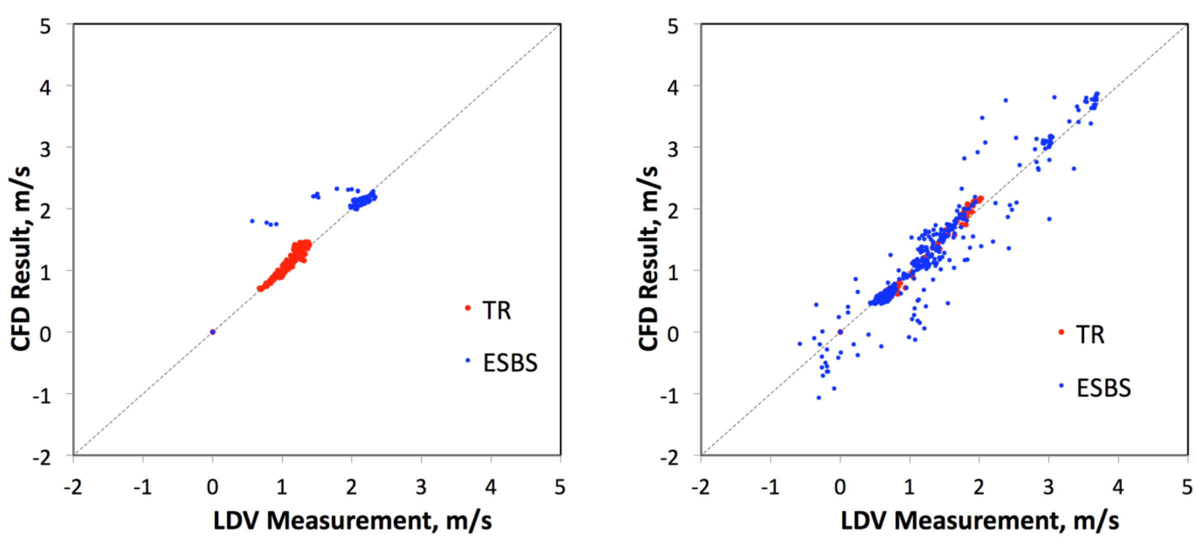

Figure 4.1. Scatter plots of one-to-one comparisons between velocities (stream-wise direction) from CFD (PNNL) and LDV data (ERDC) for the AB1-nE (left) and the AB1-wE (right) operating points. Data points are colored by location (TR = upstream locations near the trash racks; ESBS = downstream locations near the ESBS).

Figure 4.2 and Figure 4.3 show the mean velocity profiles in the vertical direction from both the laboratory measurements (ERDC) and the present CFD results. The mean values of the two velocity components (stream-wise and vertical) are plotted for those locations downstream of the ESBS. Each subplot consists of four measurement lines of Bay A (the only bay measured and shown in Figure 4.3, left). The comparisons between data show a better agreement for the stream-wise component in both operating points than for the vertical component. The vertical component shows a stronger lateral variability for the LDV data than for the CFD results. For the AB1-wE operating point, the comparisons reveal a slight underestimation of the ESBS blockage effect, as shown by the lower gradients of stream-wise velocities from the CFD results. This discrepancy could be corrected by an iterative increment in resistance coefficients for the screen and perforated plates until a closer agreement is obtained; however, the strategy implemented in this modeling work consisted of applying localized coefficients for each resistance rather than adjusting parameters to match laboratory data. The vertical velocities were for the most part negative.

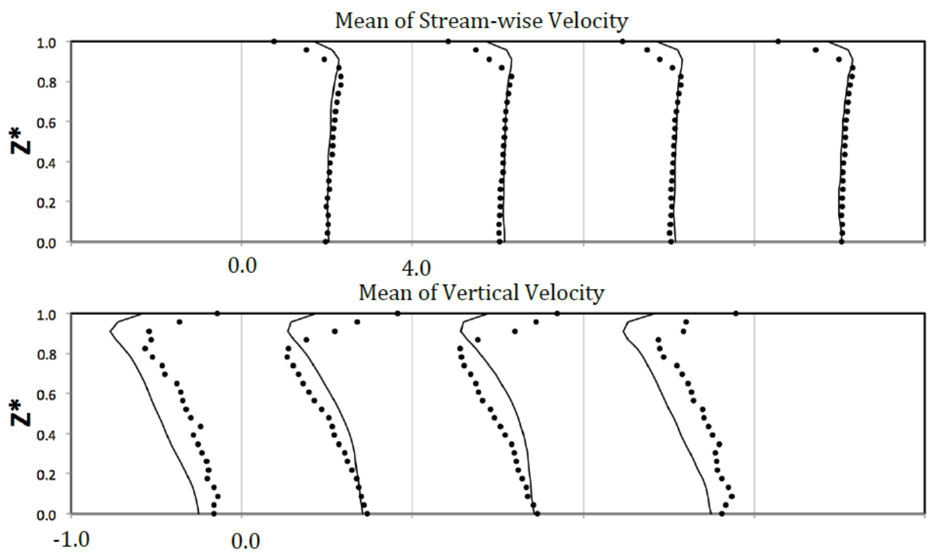

Figure 4.2. Vertical distribution of both the stream-wise and vertical velocities (in m/s) at the LDV measurement locations downstream from the ESBS, for the AB1-nE operating point (ERDC = filled circles; CFD = continuous line).

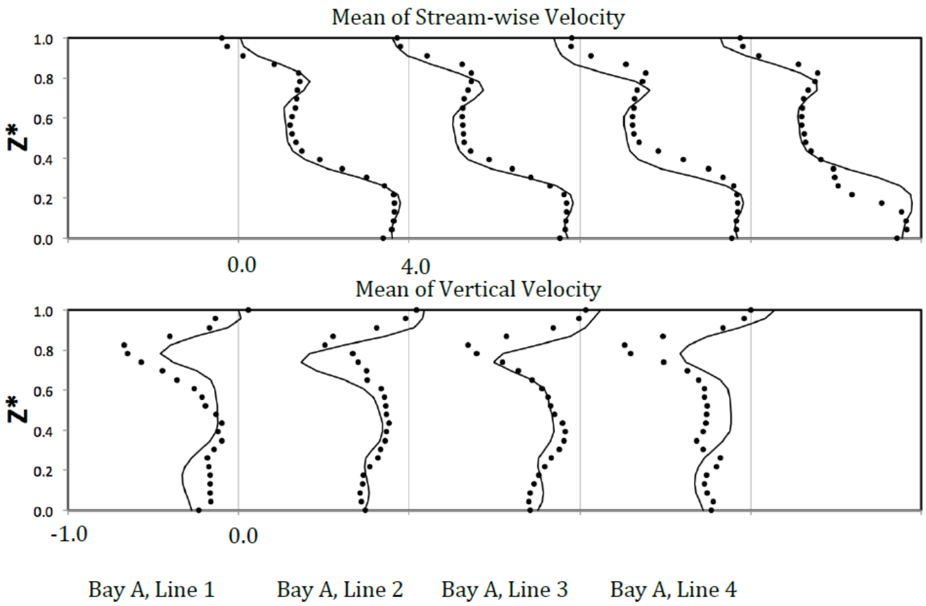

Figure 4.3. Vertical distribution of both the stream-wise and vertical velocities (in m/s) at the LDV measurement locations downstream from the ESBS, for the AB1-wE operating point (ERDC = filled circles; CFD = continuous line).

Vector plots in Figure 4.4 correspond to Line 2 in Bay A of the AB1-wE operating point. The level of agreement among these data sources increases confidence in the accuracy of the CFD modeling work in the intake region of the turbine unit. Particularly, the upstream data points (near the trash racks) showed a considerable agreement at the point where the flow begins to deflect owing to the presence of the ESBS resistances. This indicates that the selection of the resistance coefficients is adequate to obtain an acceptable description of the flow fields in the presence of a strong blockage effect. The disagreement in the upper portion of the downstream measurement points is related to the modeling limitation to represent the strong flow recirculation behind the ESBS. It is hypothesized that turbulence-resolving techniques with the ability to better represent the anisotropic conditions of turbulence (such as detached-eddy simulation) could potentially improve the agreement between data and CFD results in that zone.

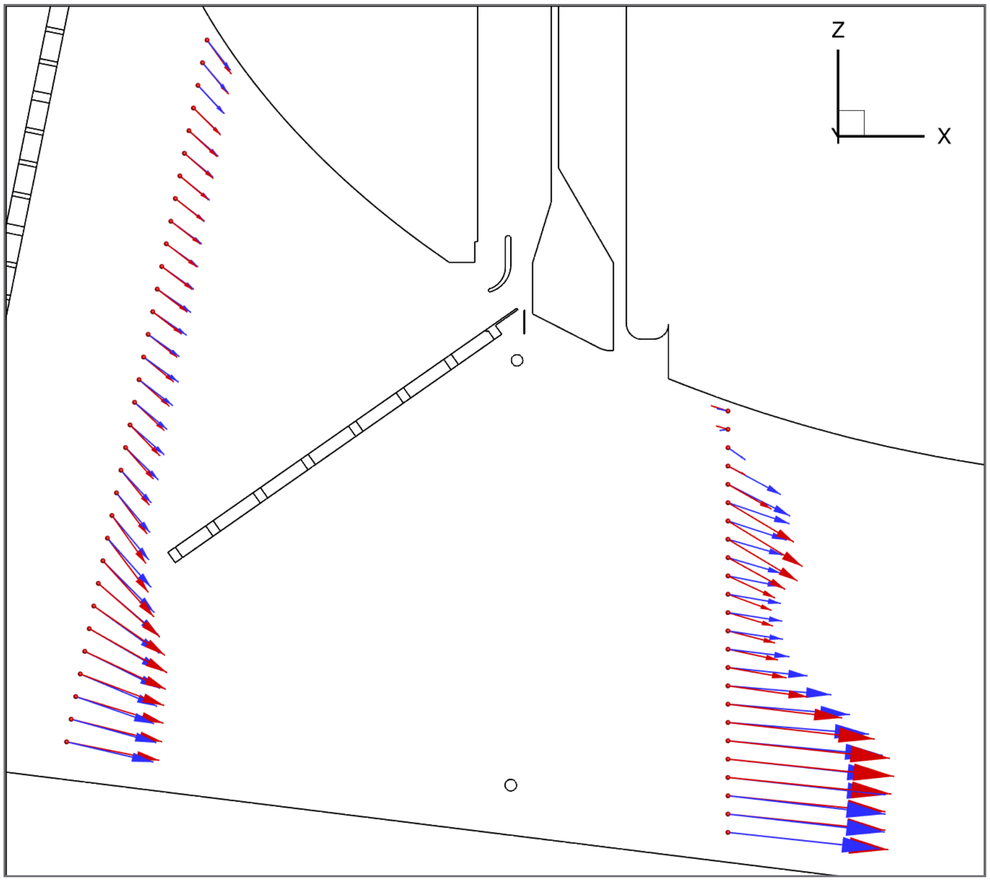

Figure 4.4. Vector plots of Line 2, Bay A for the operating point AB1-wE. CFD data are in red, LDV data are in blue.

4.1.3 Comparison to Reduced-Scale Models

Table 4.2 summarizes the comparison of discharge and power results between CFD models run at prototype scale and models run at a 1:25 reduced scale. As expected, 1:25 model results show somewhat lower values of power and discharge. This is in agreement with the trend expected because the Reynolds numbers in the 1:25 models are smaller than the prototype values. Viscous effects (resistance) will be larger in the 1:25 scale CFD models (and laboratory physical models) because the Reynolds numbers are lower than in the prototype, leading to increased energy losses and reduced values of discharge and power for a specified gross head. The trend for larger viscous effects at 1:25 scale would also affect flow through the ESBS where the screen material is represented as a porous screen.

Figure 4.5 compares absolute pressure near the runner for two model cases, ERDC-UP1-nE-GH76 and ERDC-UP1-wE-GH76. Upstream of the runner, prototype, and reduced-scale values are nearly identical. Small differences do occur below the runner, particularly in the case with the ESBS installed, where pressures in the 1:25 model are slightly higher than in the prototype model. These differences, again, reflect the increased viscous effects of the reduced-scale models. The impact of this effect was greater in the with-ESBS case as evidenced by the larger discrepancy in power values between the prototype and 1:25 scale model results (see Table 4.2). Higher pressures in the 1:25 scale models also result in slightly higher BioPA scores for nadir pressure (see Table 4.3).

Table 4.2. Hydraulic performance comparisons between prototype- and 1:25-scale CFD models.

Model	Discharge (cfs) Meas.	CFD	Δ	Δ1:25	Power (hp) Target	CFD	Δ	Δ1:25
ERDC-UP1-nE-GH73	12,560	11,431	-1,129	-9	89,300	84,280	-5,020	-1890
ERDC-UP1-nE-GH73-1to25	12,560	11,422	-1,138		89,300	82,390	-6,910	
ERDC-14500-nE-GH73	14,620	13,717	-903	-95	-	100,072	-	-3988
ERDC-14500-nE-GH73-1to25	14,620	13,622	-998		-	96,084	-	
ERDC-PEAK-nE-GH76	9,940	9,478	-462	-98	76,000	71,765	-4,235	-3431
ERDC-PEAK-nE-GH76-1to25	9,940	9,380	-560		76,000	68,334	-7,666	
ERDC-UP1-nE-GH76	12,525	12,076	-449	-7	92,900	92,917	17	-1639
ERDC-UP1-nE-GH76-1to25	12,525	12,069	-456		92,900	91,278	-1,622	
ERDC-UP1-wE-GH76	12,525	11,924	-601	-155	90,900	85,192	-5,708	-4486
ERDC-UP1-wE-GH76-1to25	12,525	11,769	-756		90,900	80,706	-10,194	

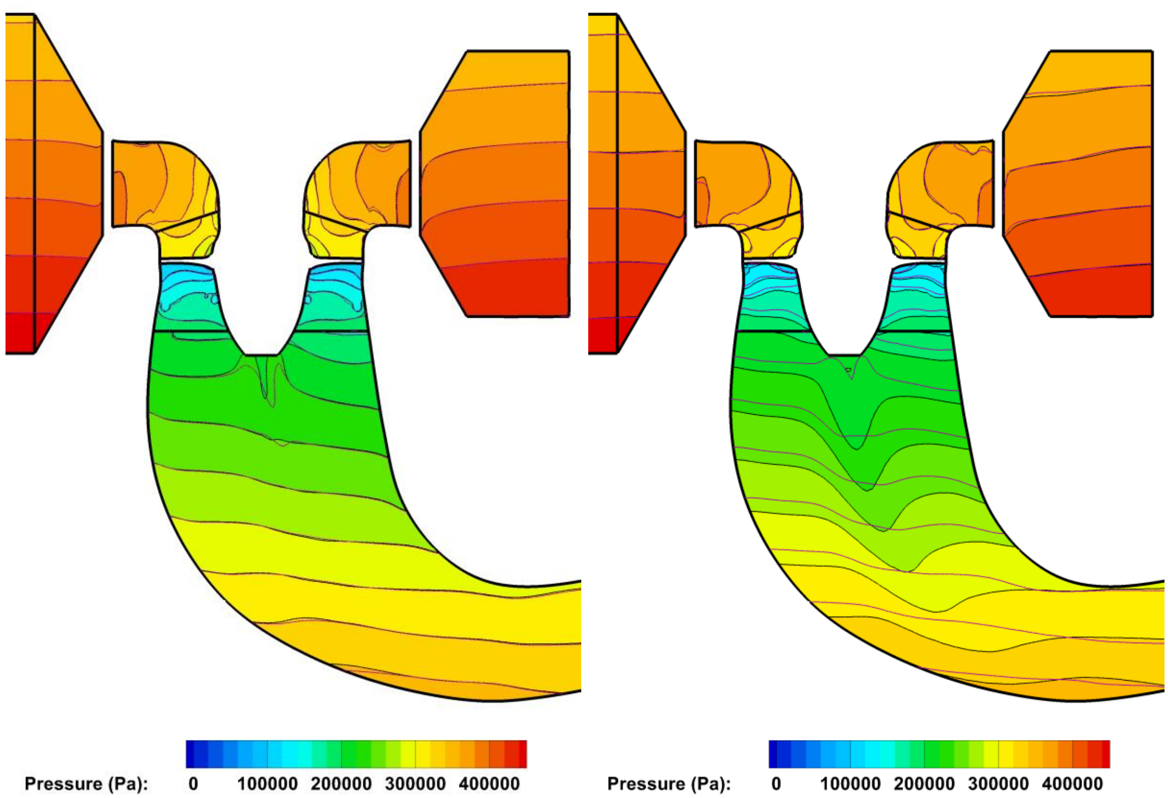

Figure 4.5. Comparison of absolute pressure between prototype-scale models (colored flood contours with black lines) and 1:25 scale models (purple contour lines). Condition ERDC-UP1-nE-GH76 is on left; ERDC-UP1-wE-GH76 is on right.

Table 4.3. BioPA metrics for selected 1:25 scale operating cases.

Model	Discharge (kcfs)	Power (hp)	Scale	PQI_{NP}	$10\%ile_{NP}$ (psi)	%NP<1atm (%)
PEAK-nE-GH76	9,478	71,765	proto	493	19.6	1%
			1:25	496	20.3	0%
UP1-nE-GH76	12,076	92,917	proto	488	15.2	12%
			1:25	488	15.2	14%
UP1-wE-GH76	11,924	85,192	proto	486	15.2	13%
			1:25	492	16.0	5%

4.2 BioPA Results

BioPA PQIs were computed for the DIST and VERT seed populations and are shown in Table 4.4 and plotted in Figure 4.6 (both in Section 4.2.2.2). In addition to PQI scores, the BioPA provides information about the locations of nadir pressure stressor maxima and other comparison metrics. The following sections summarize BioPA results, beginning with streamtrace premature termination rates. Next, results for pressure are summarized. Finally, differences between the two seed populations are presented.

4.2.1 Streamtrace Premature Termination Rate

A fraction of the streamtraces generated at the seed locations terminated before reaching the end of the draft tube in the model. This generally occurs when paths encounter regions of zero velocity close to walls. A premature termination rate of about 5% is typically observed in BioPA turbine studies, including this one, and is considered acceptable as long as the failed streamtraces are randomly dispersed so that they do not bias the results. Figure 4.6 shows an example of the intake seed array with seeds for prematurely terminating streamtraces blanked out.

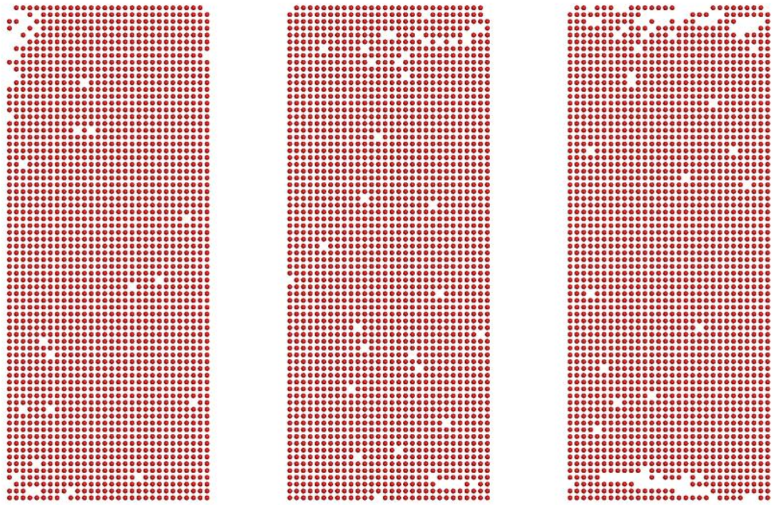

Figure 4.6. Example showing intake seed plane with seeds for prematurely terminating streamtraces blanked out.

4.2.2 Nadir Pressure

The BioPA process produced several types of data useful for characterizing and comparing pressure in the turbine environment. In addition to PQI_{NP}, the metrics *%NP<1atm* and $10\%ile_{NP}$ were computed. Locations and frequency distributions of nadir pressures were also generated.

Results from this BioPA for MCN study showed many of the trends in pressure distributions and nadir values typical of similar studies conducted by PNNL for other Kaplan turbines (e.g., Ice Harbor Dam [Serkowski et al. 2016] and Priest Rapids Dam).

4.2.2.1 Nadir-Pressure Metrics

The three nadir-pressure metrics used in this study—PQI_{NP}, *%NP<1atm*, and $10\%ile_{NP}$—are summarized in Table 4.4 and plotted in Figure 4.7. PQI_{NP} scores generally decrease with increasing discharge. The metrics *%NP<1atm* and $10\%ile_{NP}$ show similar trends with respect to discharge.

4.2.2.2 Nadir-Pressure Locations

The BioPA software generates plots of the locations where nadir pressures occur for each trajectory through the turbine. This information can help identify regions where the lowest pressures are likely occurring. Appendix A contains plots of nadir-pressure locations for the DIST population for each model. All nadir-pressure locations in the turbine models occur at or below the runner blades. These locations may be classified into three distinct regions, as shown in Figure 4.8:

- under blade: under the middle of the runner blades
- at the blade tip: in the gaps between the outer blade edge and the discharge ring
- at the blade leading edge: along the lower side of the leading edge of the blade.

The undersides of runner blades typically experience some of the lowest pressures in the turbine, so examination of these surfaces is an effective way of visualizing important differences among the operations. Appendix B contains plots of the absolute pressures on the suction (under) side of the runner blades for each model. The vast majority of nadirs occur under the middle of the runner blades. In this region, nadir pressures decrease as trajectories pass closer to the suction side of the blade.

Table 4.4. BioPA metrics for primary operating cases.

Model	Discharge (cfs)	Power (hp)	Population	PQI_{NP}	$10\%ile_{NP}$ (psi)	%NP<1atm (%)
PEAK-nE-GH76	9,443	73,119	DIST	493	19.6	1%
			VERTnE	496	19.6	1%
UP1-nE-GH76	12,083	92,976	DIST	488	15.2	12%
			VERTnE	490	16.0	9%
AB1-nE-GH76	14,489	110,562	DIST	464	10.2	38%
			VERTnE	460	9.4	37%
PROP-nE-GH73	15,833	114,232	DIST	458	9.4	39%
			VERTnE	451	8.7	38%
UP1-wE-GH76	11,872	89,637	DIST	486	15.2	13%
			VERTwE	489	16.7	5%
AB1-wE-GH76	14,188	104,870	DIST	467	10.2	37%
			VERTwE	477	12.3	28%

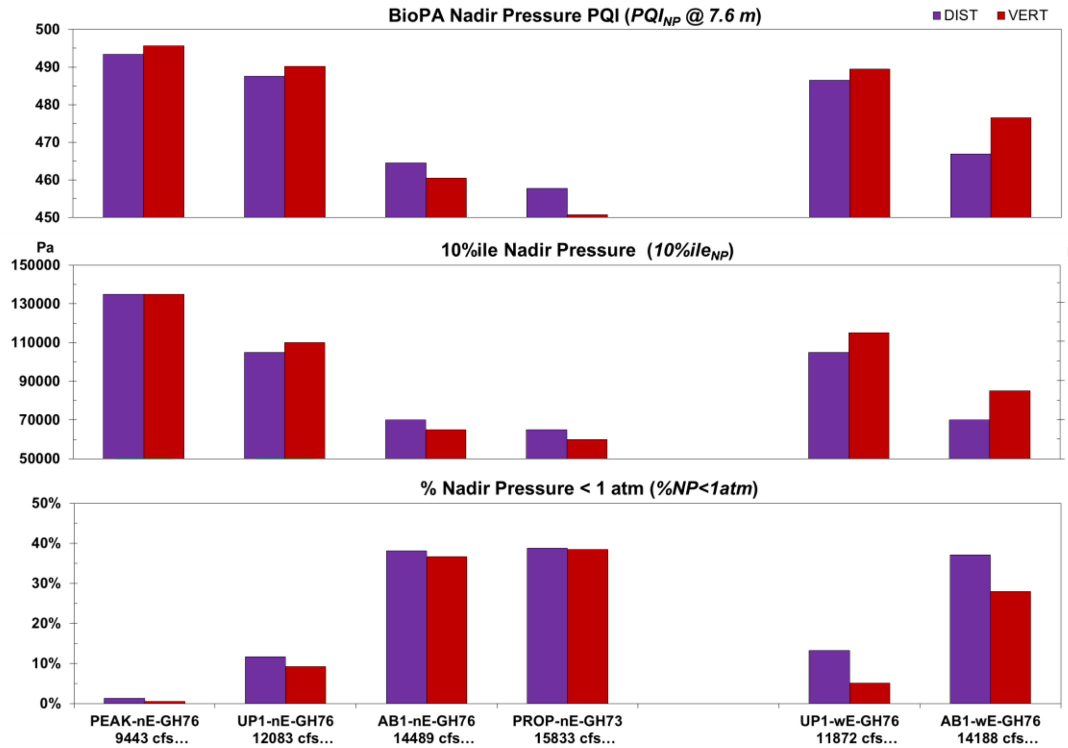

Figure 4.7. DIST (violet) and VERT (red) population nadir-pressure metrics for the prescribed operating cases.

The very lowest pressures occur on the blade tips and the blade leading edges. Many of the nadirs in the DIST population occur in one of these two locations (Figure 4.9). The relative frequency of nadirs at the blade tip tends to decrease with increasing discharge, while at the blade leading edge it increases.

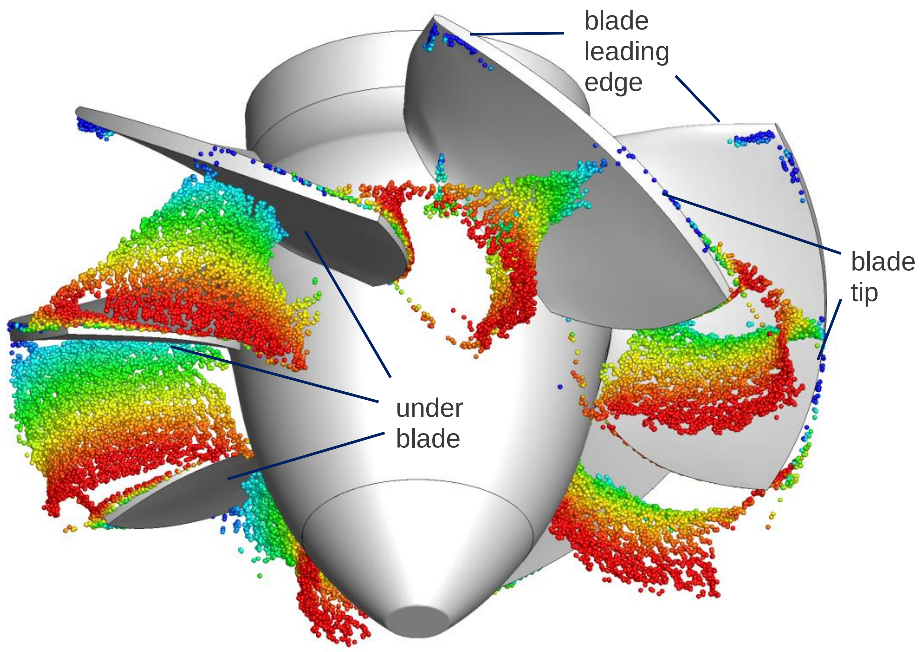

Figure 4.8. Typical nadir pressure locations; blue points have the lowest values.

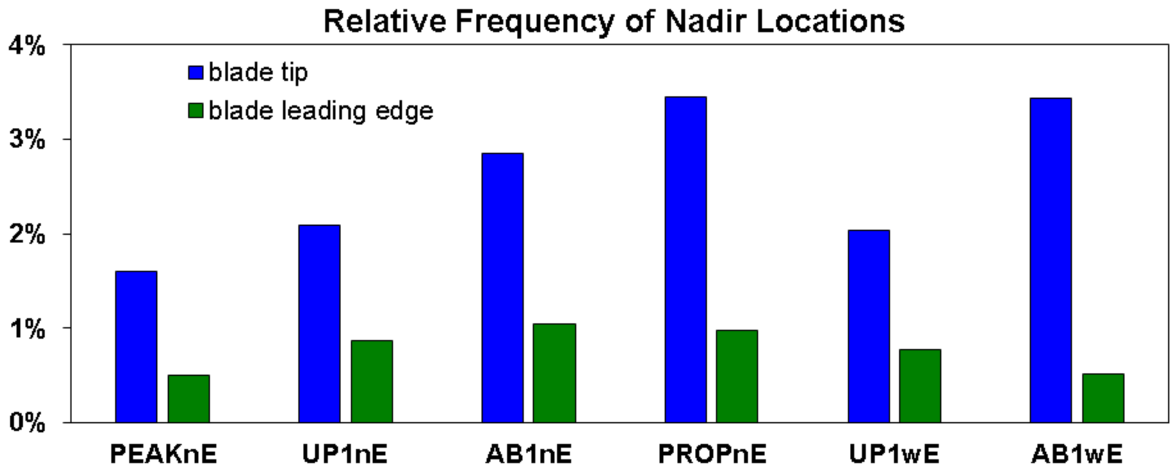

Figure 4.9. Relative frequency of DIST population nadir locations.

4.2.2.3 Nadir-Pressure Distributions

The shape of the nadir-pressure frequency distribution curve is critical to the evaluation of biological effects. Nadir-pressure distributions for the five prescribed operations for the DIST and VERT populations are plotted in Appendix C. Distribution percentiles are plotted in box-and-whisker style, and distributions are presented using incremental and cumulative frequency plots.

Several trends, all related to discharge, are apparent in these data. Nadir-pressure medians (50th percentile values in the box-and-whiskers plots) and modes (tallest points of curves in frequency distribution plots) decrease with increasing discharge. This general trend is expected from the Bernoulli equation. Moreover, the spread in the distributions, as expressed by taller boxes and wider whiskers, also increases with discharge, indicating greater pressure variability in the higher-flow cases. The general shape of the incremental distribution curves is similar across all operations: asymmetrical with the mode toward the higher-pressure side. As discharge increases, the modes move to the left (lower pressures) and the left-side tail extends farther from the mode. The width of the tails on the right sides of the modes do not change appreciably between the operations.

Note that incremental distributions for the higher-discharge models include a small fraction of near-zero nadir pressures (see, for example, the lower-left plot in Figure C.1). The presence of this “bump” is an artifact of the CFD modeling technique. Because the vapor phase of water is not being modeled, regions of the turbine where cavitation might be occurring can produce unrealistic negative pressures. In the current analysis, all negative pressures are set to vapor pressure, resulting in a distribution “bump” close to zero. Regions of cavitation are generally small in normally operating turbines, so the additional computational expense of two-phase modeling is not considered necessary.

4.3 Population Effects

Metrics computed for the two populations considered in this study—DIST and VERT—are shown in Table 4.4 and Figure 4.7. One difference in these two populations is that the VERT population biases sampling of the runner region by weighting more heavily the streamtraces originating just below the ESBS. The impact of this weighting at a point just above the runner is demonstrated in Figure 4.10, where the left image shows streamtrace crossing points for the DIST population and the right images show points, sized by the weighting factor, for the VERT population. The figure shows that the VERT streamtraces without the ESBS (far right image) preferentially interact with the middle and hub parts of the blade, with relatively few passages occurring near the blade tips. This is a direct consequence of the majority of the streamtraces starting at a higher elevation in the intake and entering near the top of the distributor. With the ESBS in place (middle image), runner-plane crossings are uniformly distributed from hub to tip.

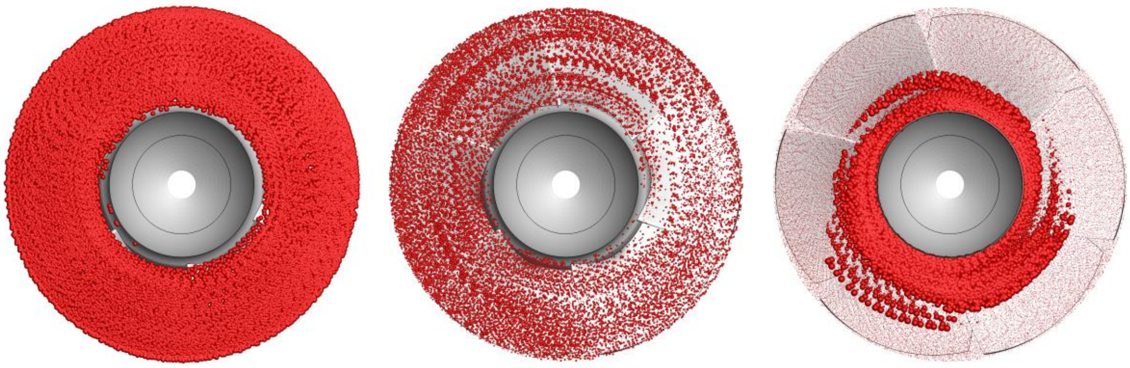

Figure 4.10. Plan views of UP1 model distribution of streamtrace crossing locations (sized by relative weighting) above the runner for the DIST (left – with ESBS), VERTwE (middle – with ESBS), and VERTnE (right – without ESBS) populations.

4.4 Runner Cone Effects

The effect of the runner cone geometry on the pressure distribution on the blades and hub is shown in Figure 4.11. Overall, the pressure values and distributions are very similar, but differences become apparent near the downstream area of the cone where the geometry differs between the actual and VAMCE cones. Similar trends were also observed for other operating points. In addition, velocities upstream of the cone geometry change experience little effect, and the velocity-dependent metrics for bead observations in the ERDC physical model would not be expected to be significantly affected in the intake, distributor, and runner. However, the cone shape does produce a different inflow condition to the draft tube and some differences were seen in the draft tube flow splits.

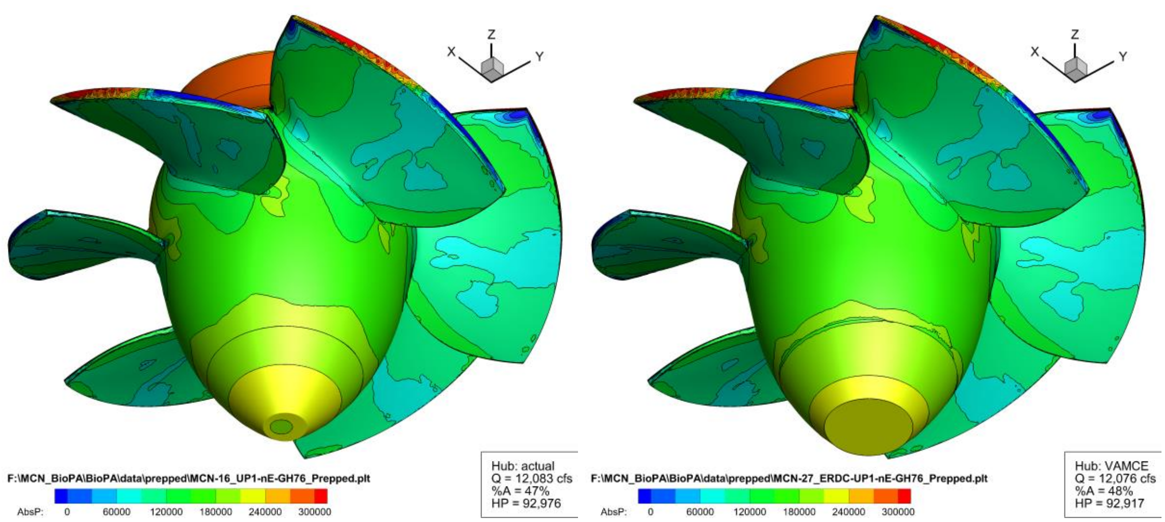

Figure 4.11. Pressures on the surface of runners with actual (left) and VAMCE (right) hub cones for UP1-nE-GH76 condition.

4.5 Draft–Tube Analysis

Figure 4.12 shows modeled velocities sampled near the draft tube exit for two example cases. The simulated MCN draft tube barrel A fraction did not follow the expected trend of having the majority of the discharge passing through barrel A as observed in the ERDC physical model (Figure 4.13). The differences in the near-exit velocity distributions shown in Figure 4.12 reflect that discrepancy in the flow splits. The general trend of barrel A having the highest discharge fraction has been observed in physical models and prior PNNL CFD simulations of other Kaplan turbine units (Figure 4.14 and Figure 4.15). The CFD modeling approach applied to the MCN turbine followed the same practice applied to Ice Harbor Dam, John Day Dam, and Priest Rapids Dam where the flow from the runner region was circumferentially averaged and then passed to the draft tube region of the model. Emerging information from the literature suggests that this approach, while widely used for Kaplan-type turbines, may be inadequate in some cases, and alternative methods that can assign a more realistic inflow may be required.

After additional examination, the draft tube flow distribution discrepancy was judged to not have an appreciable impact on the runner pressure distributions. Those pressures are predominately influenced by the total discharge, gate angle, and blade angle. But, given the unexpected results, further and more detailed analysis of the draft tube flow conditions simulated by the CFD model was not undertaken at this time.

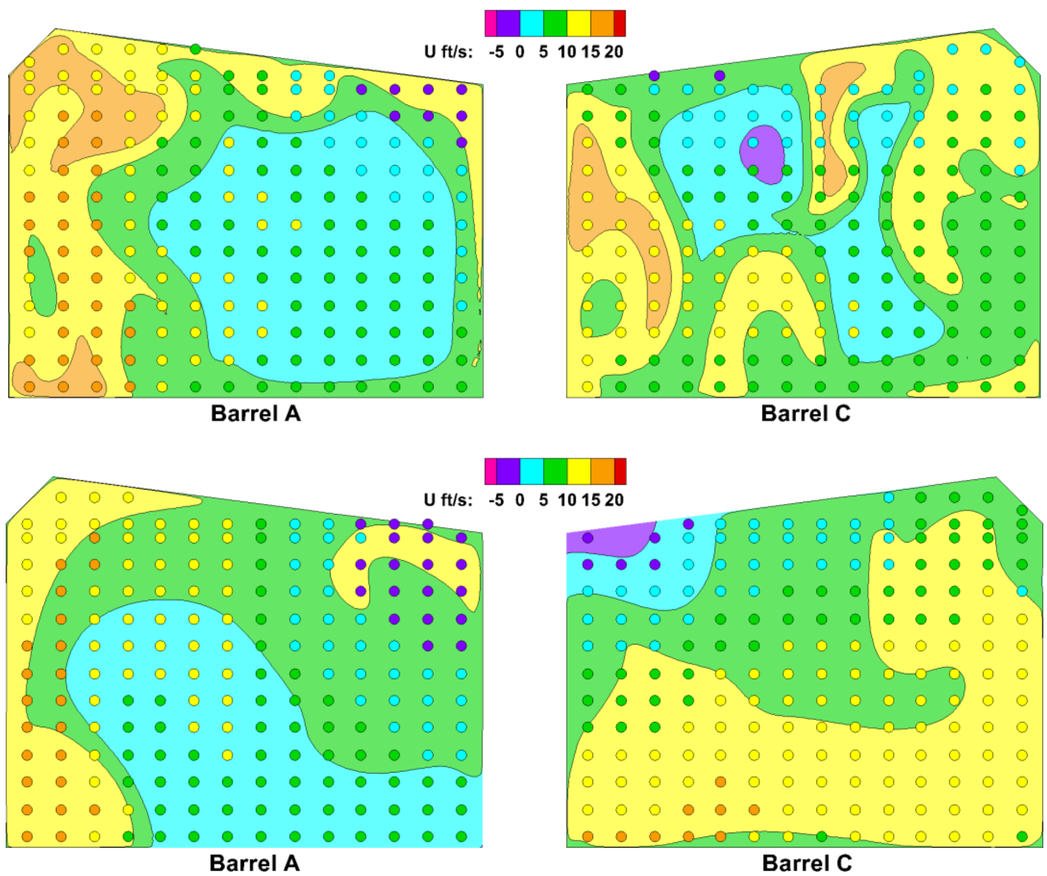

Figure 4.12. Horizontal velocity contours in the draft tube for two CFD models: ERDC-14500-wE-GH73 (top – with ESBS) and ERDC-14500-nE-GH73 (bottom – no ESBS). The sample plane is seven feet upstream of the draft tube exit and the view is looking downstream. ERDC LDV data are represented by the colored dots.

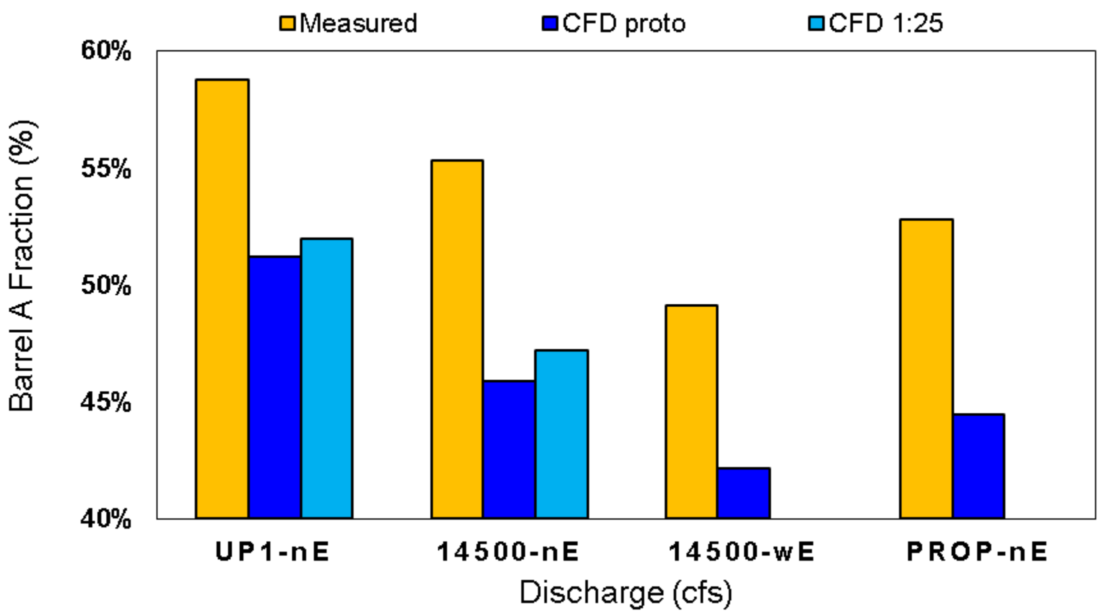

Figure 4.13. Comparison between barrel A flow fraction measured by ERDC and CFD models. All cases have a gross head of 73 ft.

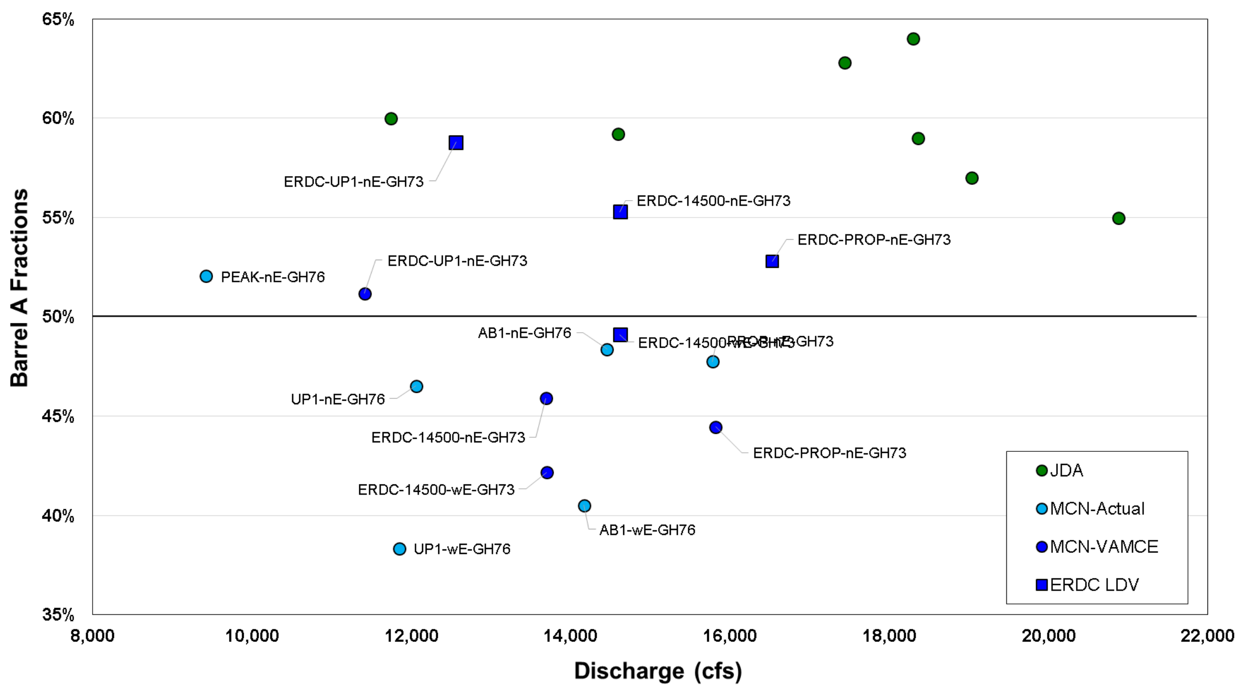

Figure 4.14. Barrel A draft-tube fraction as a function of discharge for CFD models of the John Day Dam (JDA) turbine and the MCN turbine (with actual and VAMCE cone), and ERDC LDV measurements.

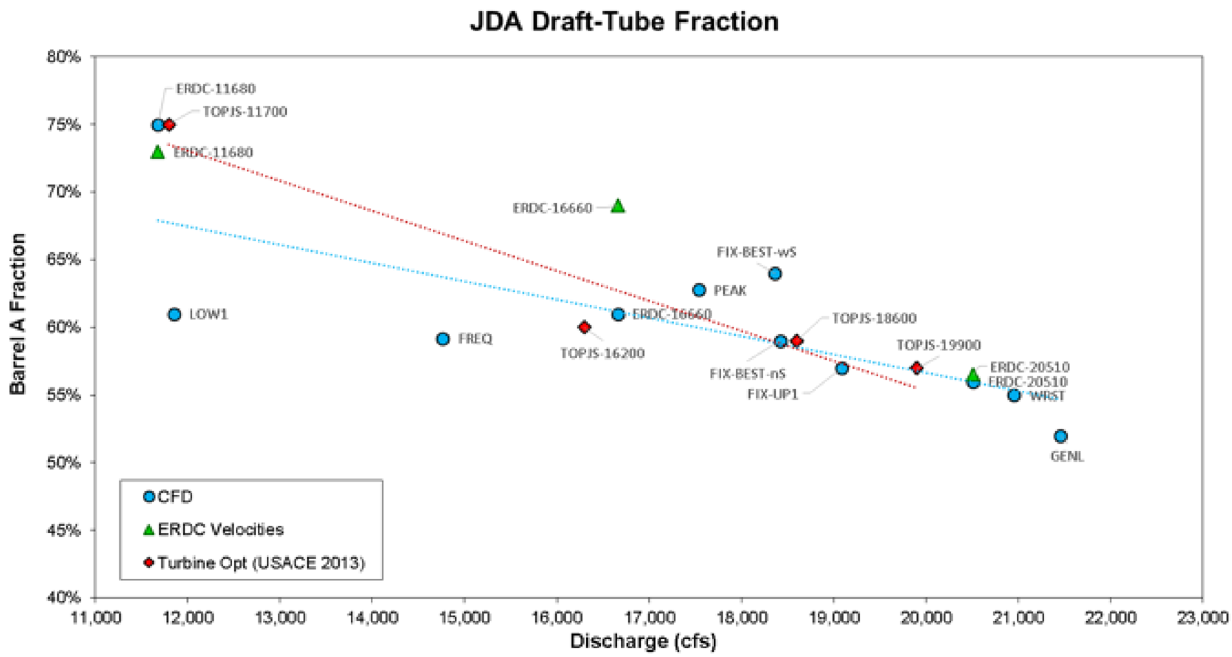

Figure 4.15. John Day existing turbine barrel A flow fraction from CFD, ERDC data, and Turbine Optimization report (red-diamonds − labeled TOPJS are from Figure 16 in "TURBINE OPTIMIZATION FOR PASSAGE OF JUVENILE SALMON AT JOHN DAY DAM"; USACE, Sept 2011).

5.0 References

Amaral SV, GE Hecker, P Stacy and DA Dixon. 2007. *Effects of Turbine Blade Thickness on Fish Injury and Survival.* In *Proceedings of 137th Annual Meeting of the American Fisheries Society AFS Bioengineering Symposium V*, San Francisco, California.

Brown RS, TJ Carlson, AJ Gingerich, JR Stephenson, BD Pflugrath, AE Welch, MJ Langeslay, ML Ahmann, RL Johnson, JR Skalski, AG Seaburg and RL Townsend. 2012. *Quantifying Mortal Injury of Juvenile Chinook Salmon Exposed to Simulated Hydro-Turbine Passage*. *Transactions of the American Fisheries Society*, 141**,** 147-157.

Deng ZD, X Li, T Fu, RS Brown, JJ Martinez, PS Titzler, JS Hughes, GA McMichael, MA Weiland, AH Colotelo, JR Skalski and RL Townsend. 2014. *Depth Distribution of Yearling and Subyearling Chinook Salmon and Juvenile Steelhead*. PNWD-4424, Prepared by Battelle Pacific Northwest Division for U.S. Army Corps of Engineers under contract number W912EF-08-D-0004.

Ghamry H and C Katopodis. 2012. *Numerical Investigation of Turbulent Flow through Bar Racks in Closed Conduits.* In *Proceedings of 9th International Symposium on Ecohydraulics*, Vienna, Austria.

Ham KD, PS Titzler and DM Trott. 2013. *Evaluation of the Effect of McNary Dam Operating Gate Position on Fish Guidance Efficiency*. PNNL-22857, Prepared by Pacific Northwest National Laboratory for U.S. Army Corps of Engineers under contract number DE-AC05-76RL01830.

Neitzel DA, MC Richmond, DD Dauble, RP Mueller, RA Moursund, CS Abernethy and GR Guensch. 2000. *Laboratory Studies on the Effects of Shear on Fish: Final Report*. DOE/ID-10822, Prepared by Idaho National Laboratory for U.S. Department of Energy.

Neitzel DA, DD Dauble, GF Čada, MC Richmond, GR Guensch, RP Mueller, CS Abernethy and BG Amidan. 2004. *Survival Estimates for Juvenile Fish Subjected to a Laboratory-Generated Shear Environment*. *Transactions of the American Fisheries Society*, 133**,** 447-454.

Odeh M, JF Noreika, A Haro, A Maynard, T Castro-Santos and GF Čada. 2002. *Evaluation of the Effects of Turbulence on the Behavior of Migratory Fish*. DOE/BP-00000022-1, Prepared by U.S. Geological Survey for Bonneville Power Administration.

Pflugrath BD, RS Brown and TJ Carlson. 2012. *Maximum Neutral Buoyancy Depth of Juvenile Chinook Salmon: Implications for Survival during Hydroturbine Passage*. *Transactions of the American Fisheries Society*, 141**,** 520-525.

Richmond MC, JA Serkowski, LL Ebner, M Sick, RS Brown and TJ Carlson. 2014. *Quantifying Barotrauma Risk to Juvenile Fish during Hydro-turbine Passage*. *Fisheries Research*, 2014**,** 152-164.

Serkowski JA, MC Richmond and PDJ Romero Gomez. 2016. *Nadir Pressure Exposure Estimates for Turbine Designs at Ice Harbor Dam*. PNNL-25455, Prepared by Pacific Northwest National Laboratory for U.S. Army Corps of Engineers.

Appendix A

Nadir-Pressure Locations for the DIST Population

Plots in this appendix show the locations of nadir pressures for the prescribed operation model cases based on the DIST population of seeds.

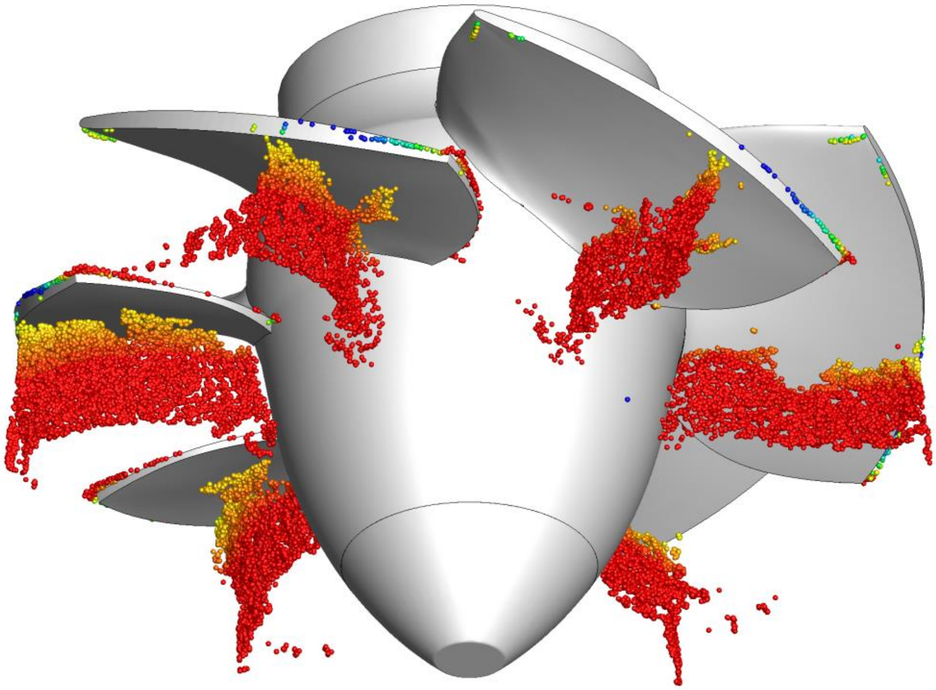

Figure A.1. PEAK-nE-GH76.

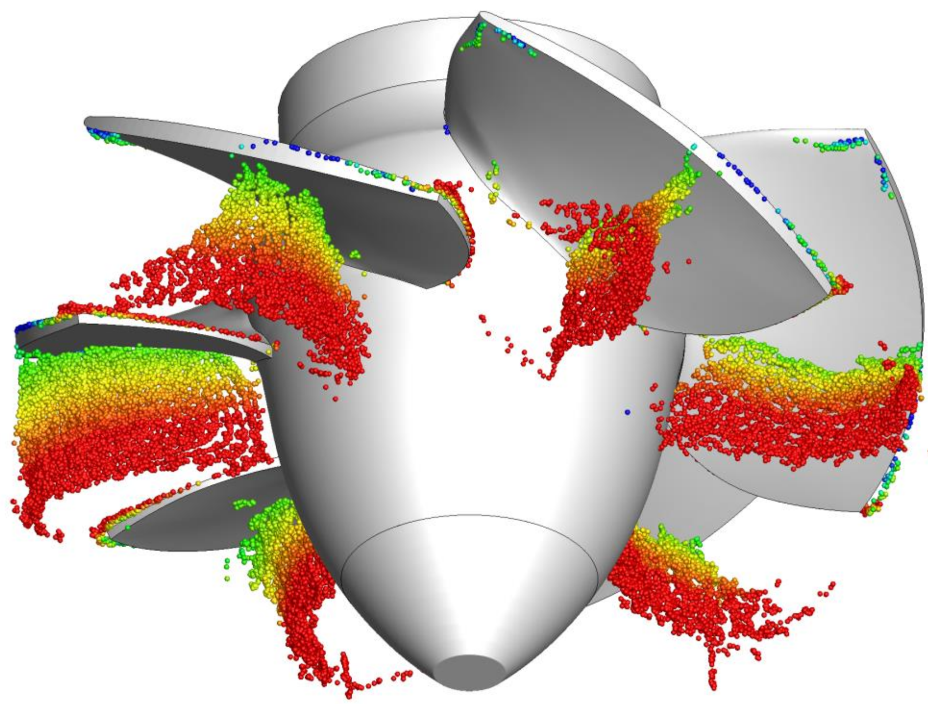

Figure A.2. UP1-nE-GH76.

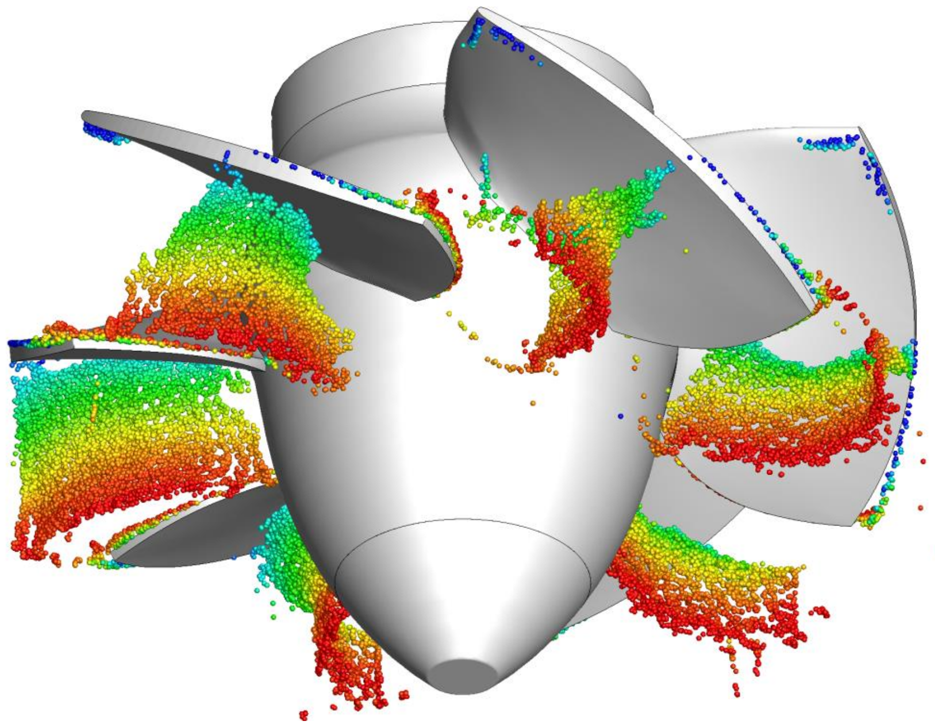

Figure A.3. MCN-14 AB1-nE-GH76.

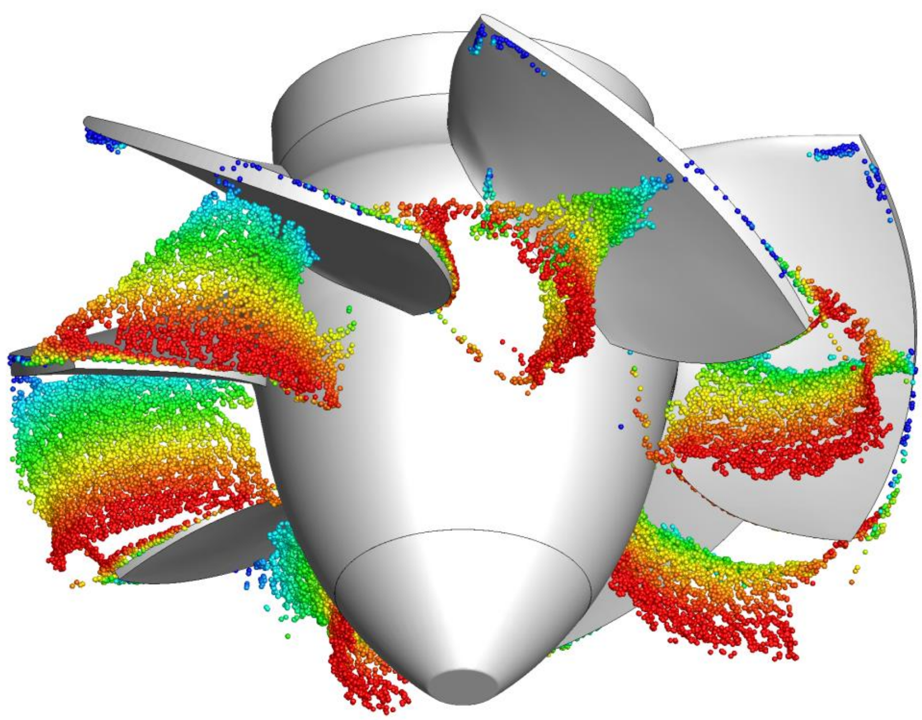

Figure A.4. PROP-nE-GH73.

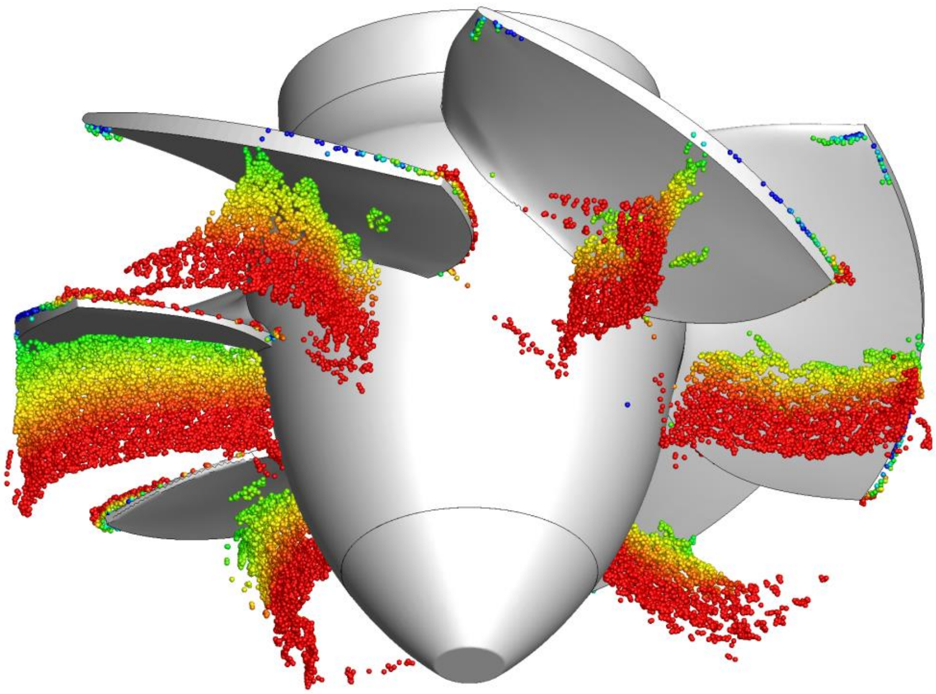

Figure A.5. MCN-18 UP1-wE-GH76.

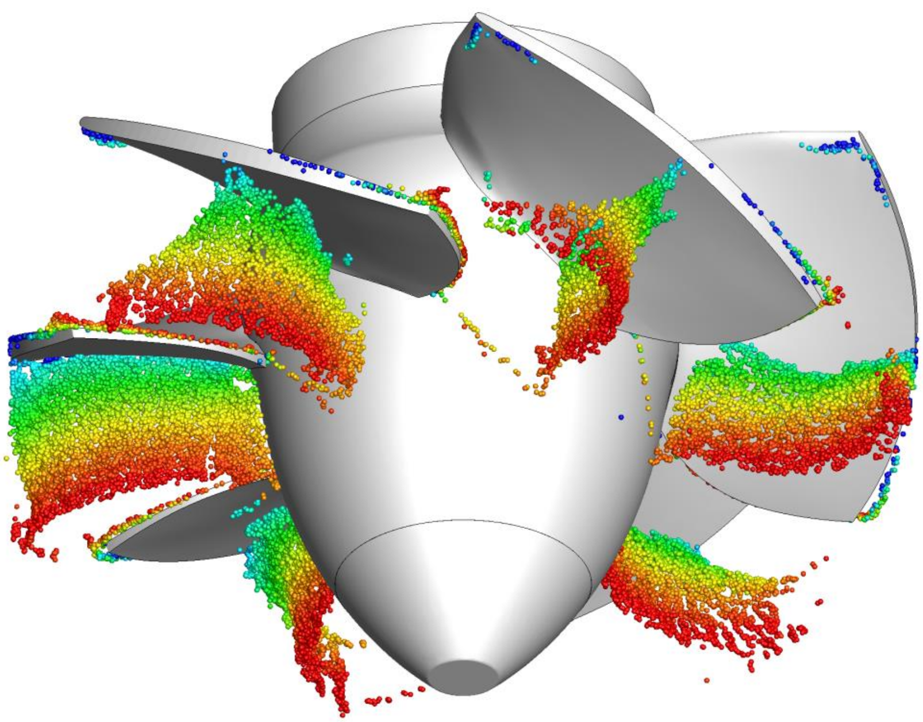

Figure A.6. MCN-15 AB1-wE-GH76.

Appendix B

Runner Suction-Side Pressure

Plots in this appendix show the absolute pressure on the underside of the runner blades for the prescribed operation model cases.

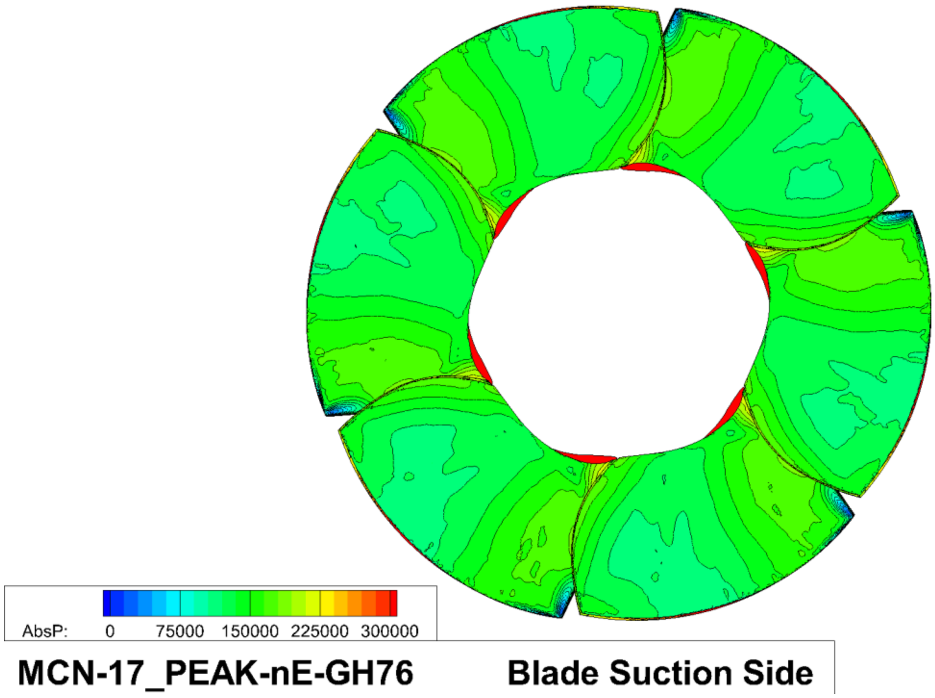

Figure B.1. Suction-side runner blade pressure for PEAK-nE-GH76.

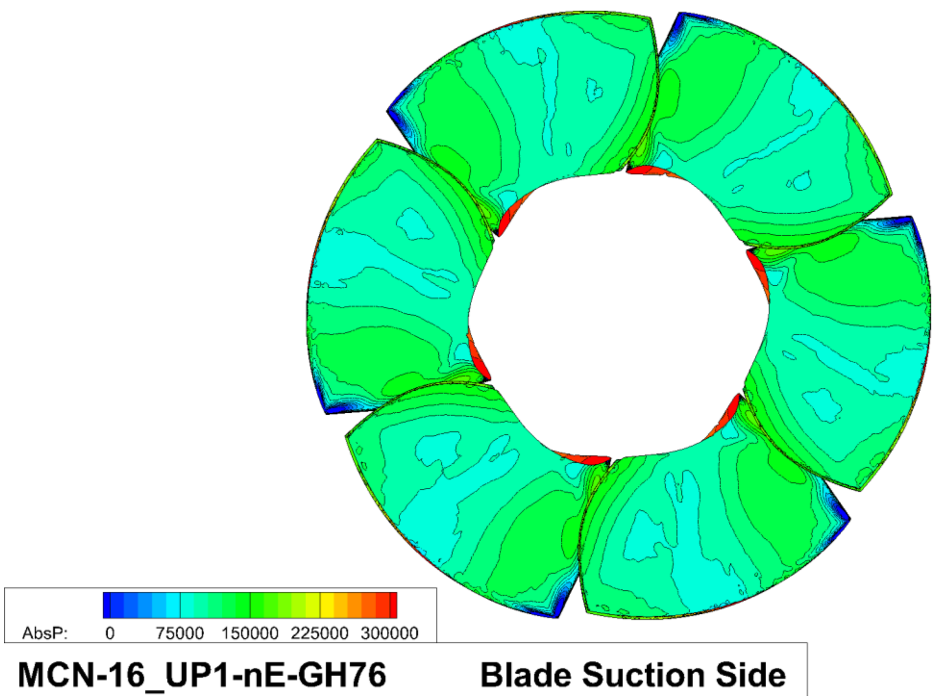

Figure B.2. Suction-side runner blade pressure for UP1-nE-GH76.

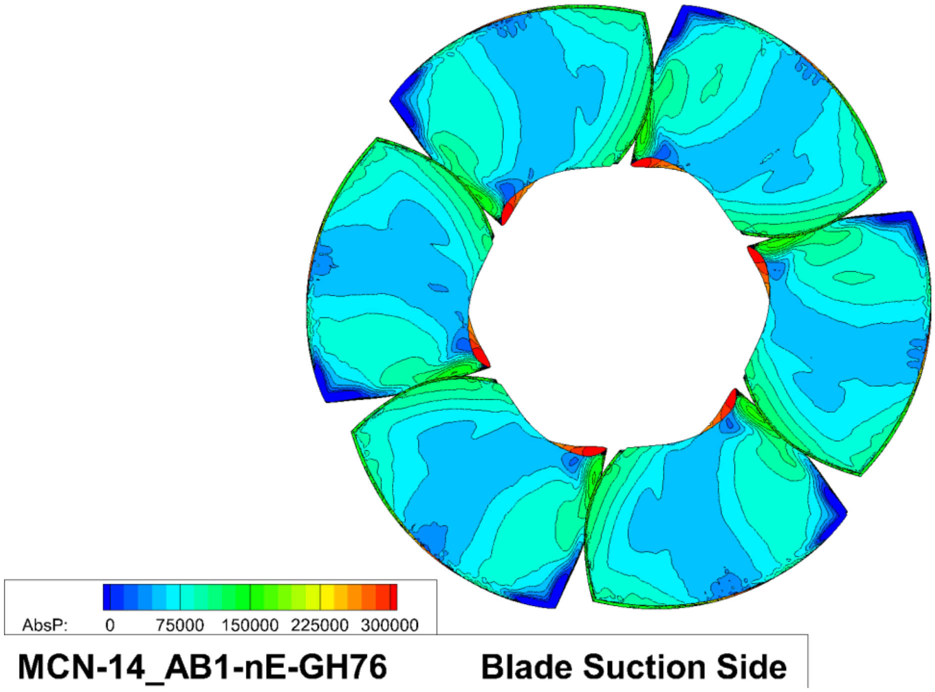

Figure B.3. Suction-side runner blade pressure for AB1-nE-GH76.

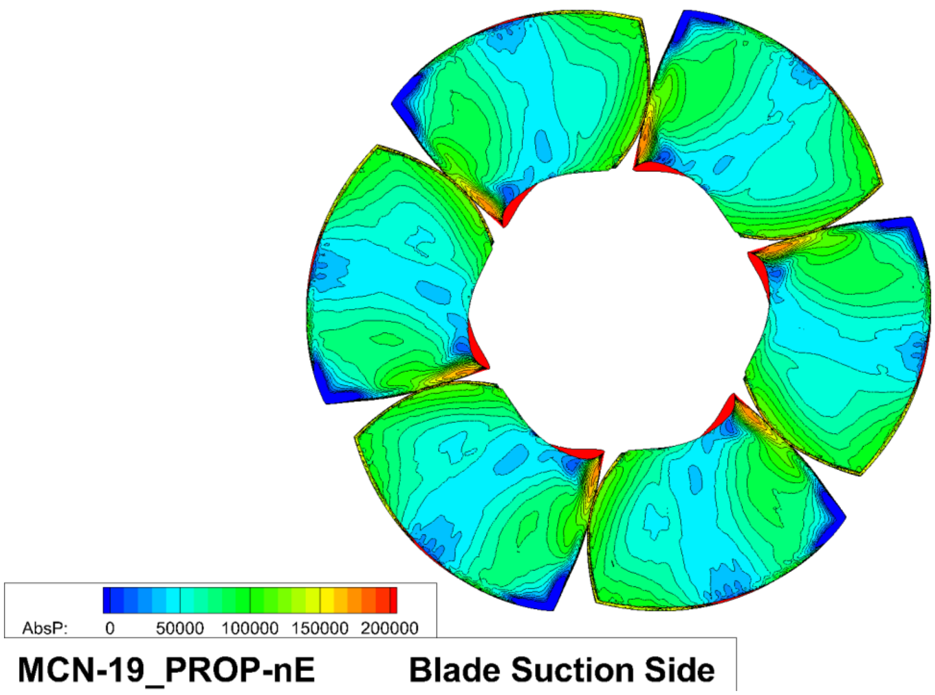

Figure B.4. Suction-side runner blade pressure for PROP-nE-GH73.

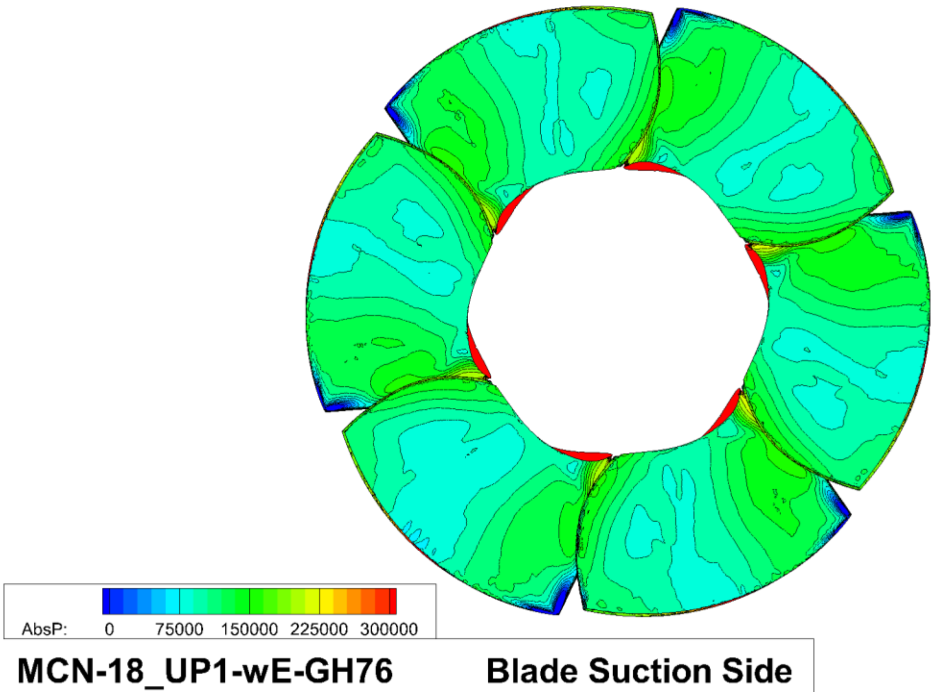

Figure B.5. Suction-side runner blade pressure for UP1-wE-GH76.

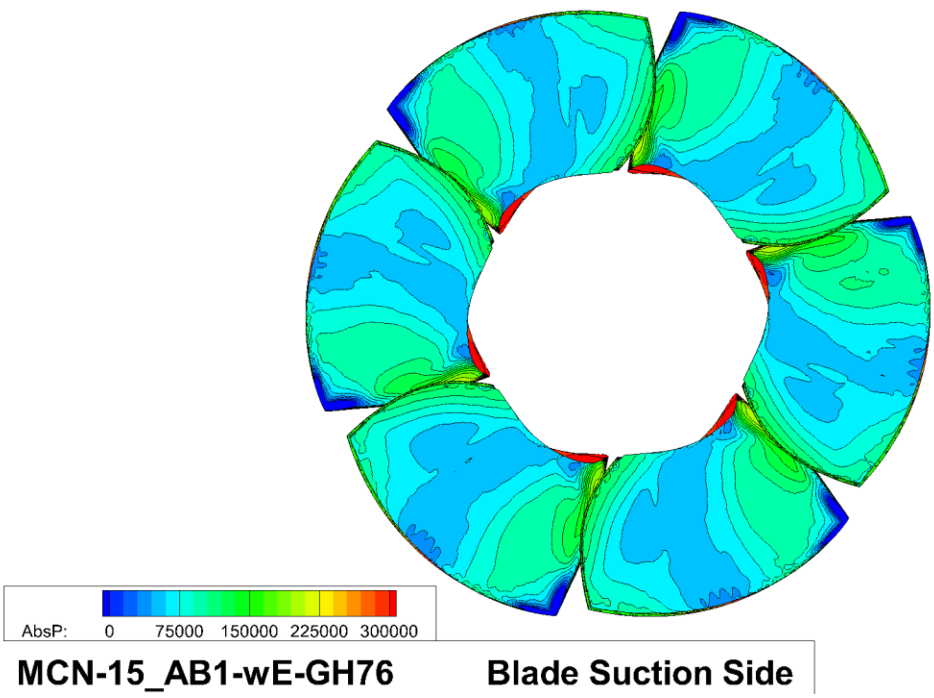

Figure B.6. Suction-side runner blade pressure for AB1-wE-GH76.

Appendix C

Nadir-Pressure Distributions for the DIST Population

Plots in this appendix summarize the frequency distributions of nadir pressures for the prescribed operations based on the DIST and VERT populations of seeds.

Three plots are shown for each comparison group:

- box-and-whiskers plot with the box defining the 25-50-75 percentiles of pressure nadirs and the whiskers the 10 and 90 percentiles
- incremental nadir-pressure distribution computed in 5,000 Pa (0.7 psi) increments
- cumulative nadir-pressure distribution computed in 5,000 Pa (0.7 psi) increments.

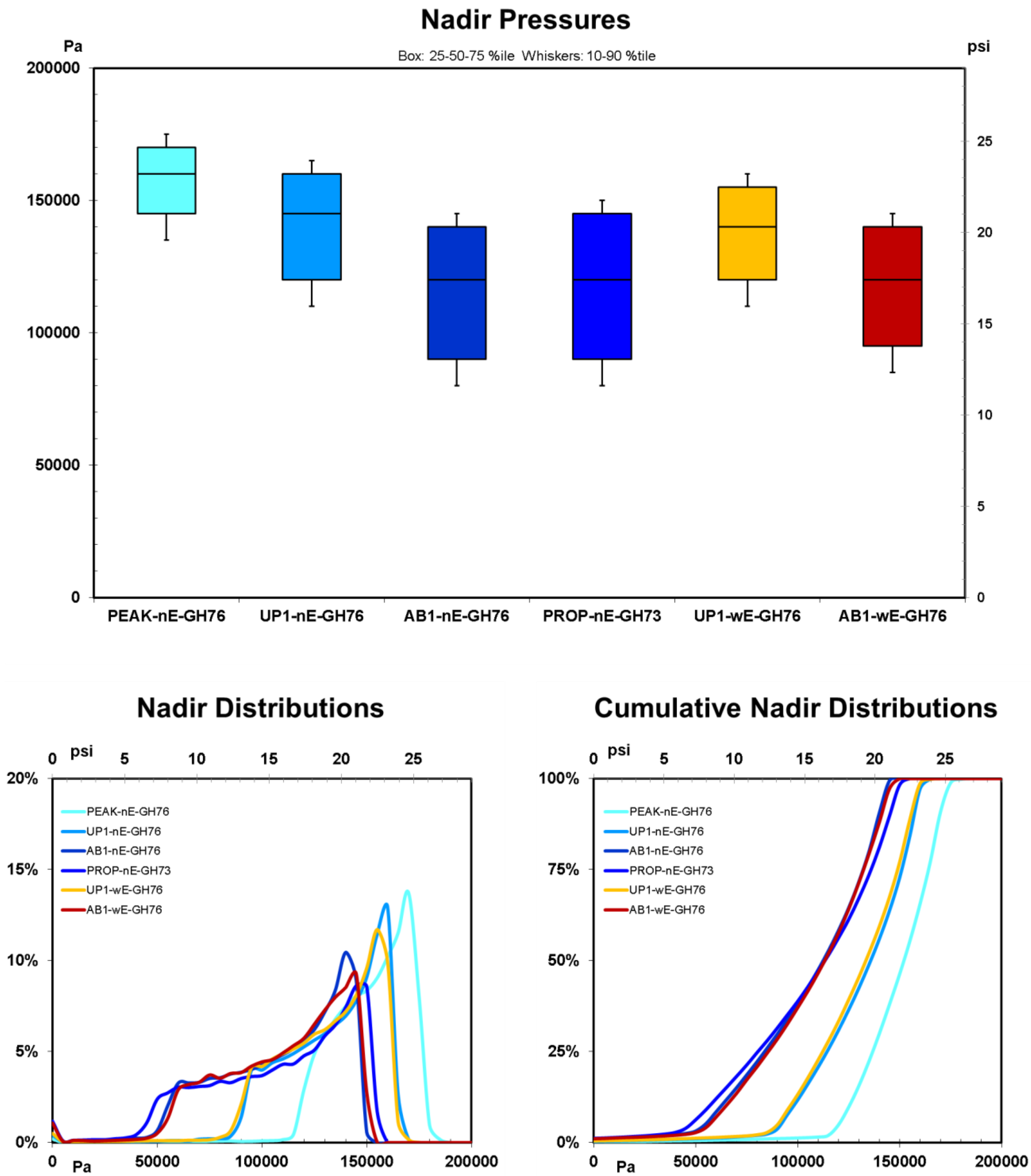

Figure C.1. Nadir-pressure distributions for DIST population.

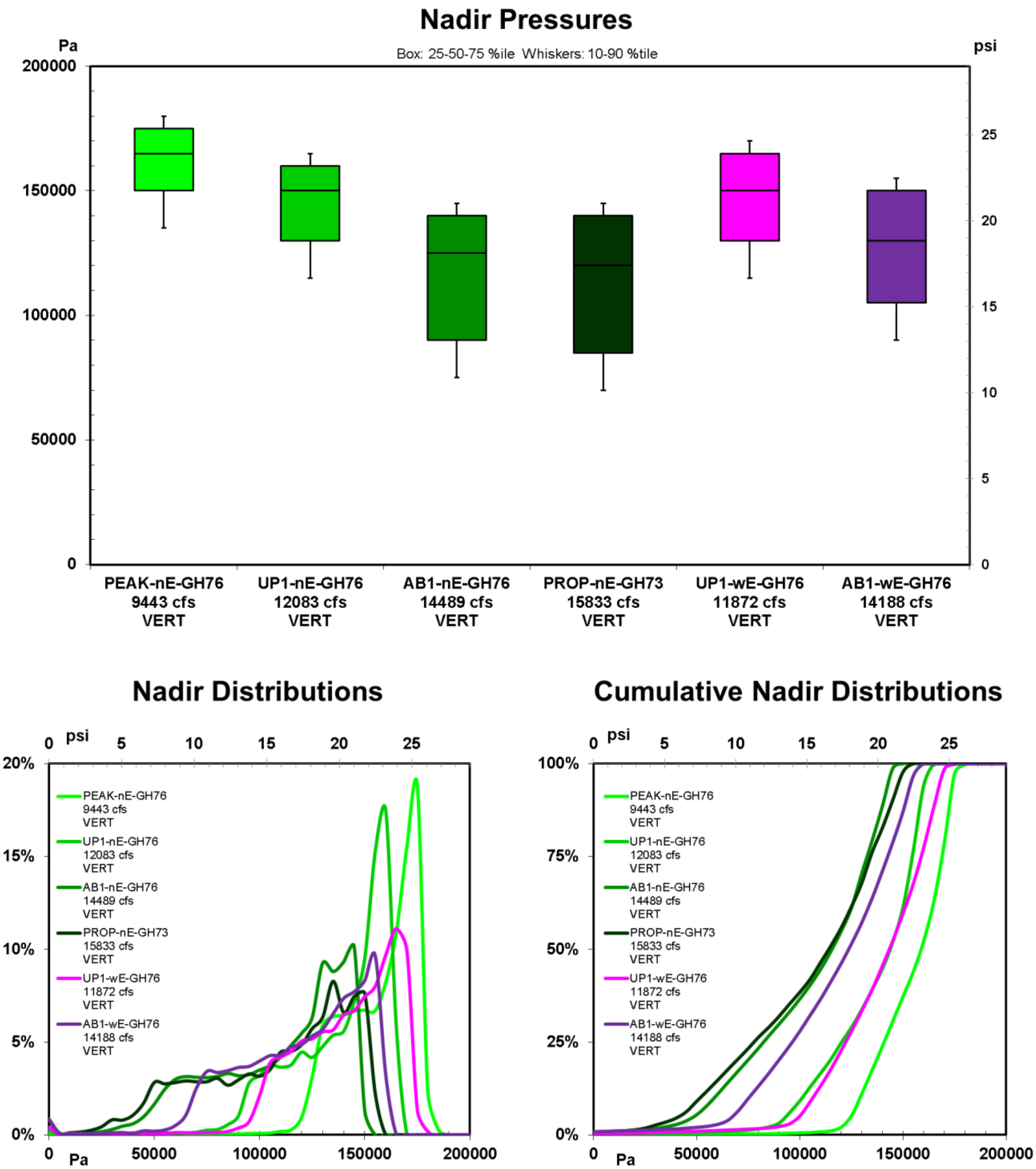

Figure C.2. Nadir-pressure distributions for VERT population.

Appendix D

Under-Runner Velocity Comparisons

Plots in this appendix present comparisons between under-runner velocity measurements collected by ERDC at their 1:25 physical model (red vectors) and corresponding velocities from CFD models run at both prototype and 1:25 scales (blue vectors).

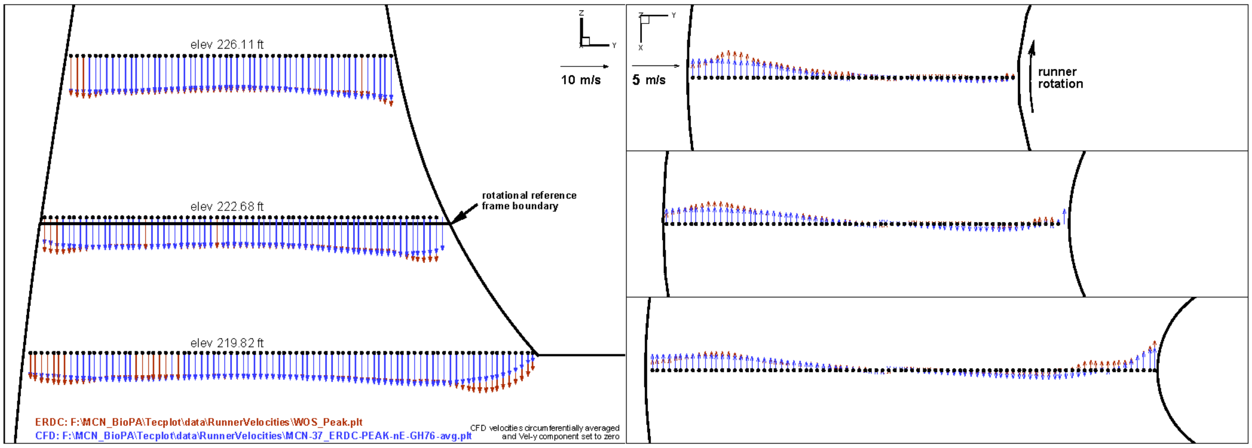

Figure D.1. Under-runner velocity comparisons for ERDC-PEAK-nE-GH76.

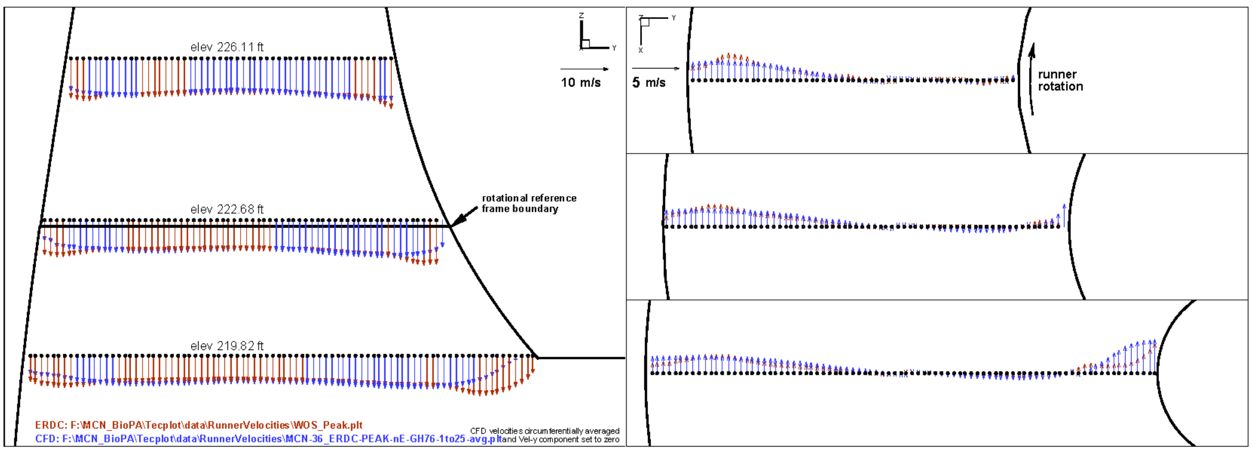

Figure D.2. Under-runner velocity comparisons for ERDC-PEAK-nE-GH76-1to25.

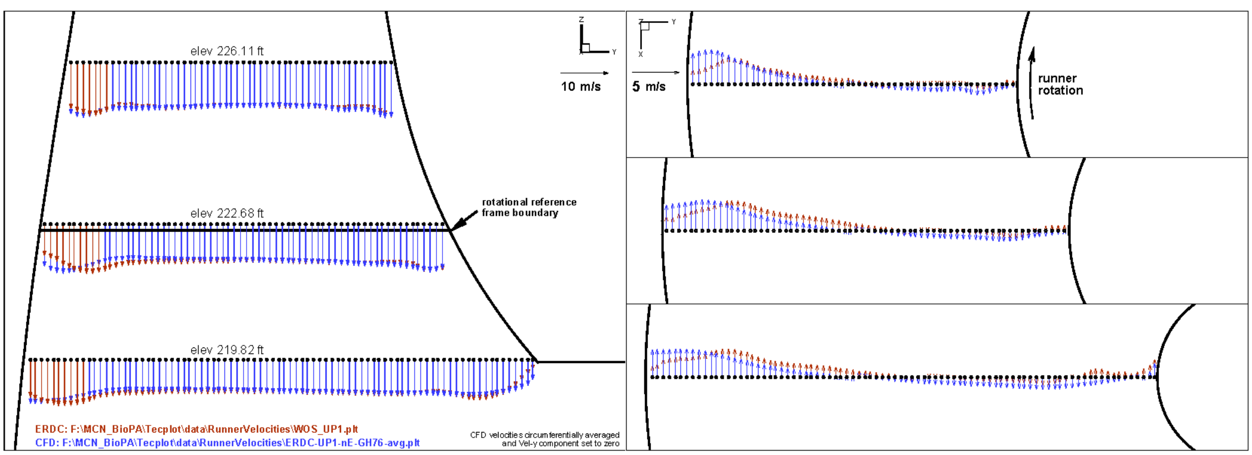

Figure D.3. Under-runner velocity comparisons for ERDC-PEAK-nE-GH76.

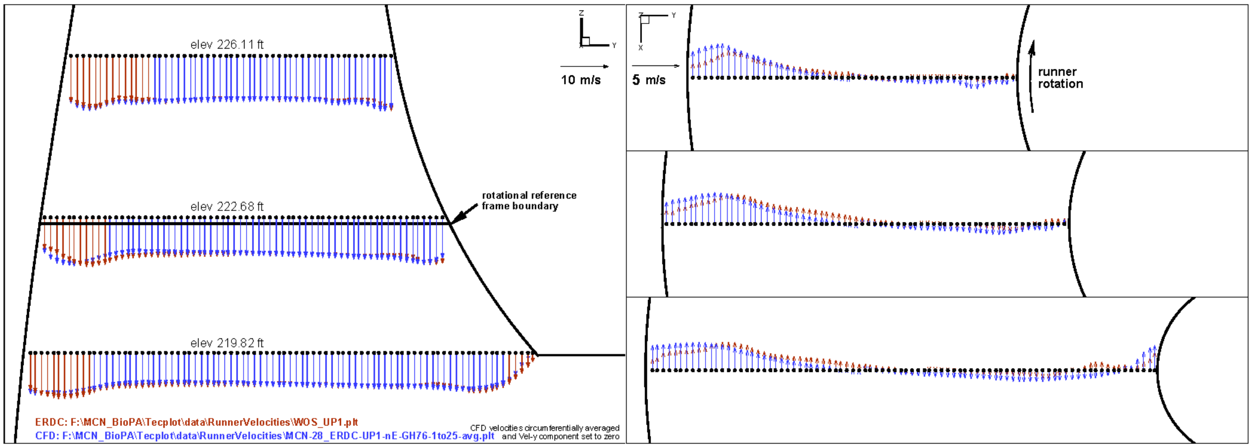

Figure D.4. Under-runner velocity comparisons for ERDC-UP1-nE-GH76-1to25.

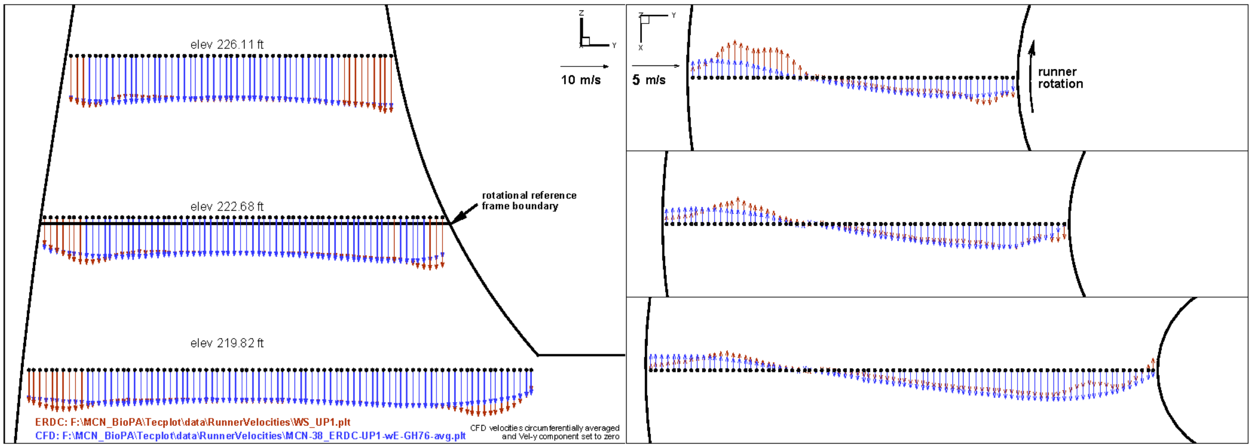

Figure D.5. -runner velocity comparisons for ERDC-UP1-wE-GH76.

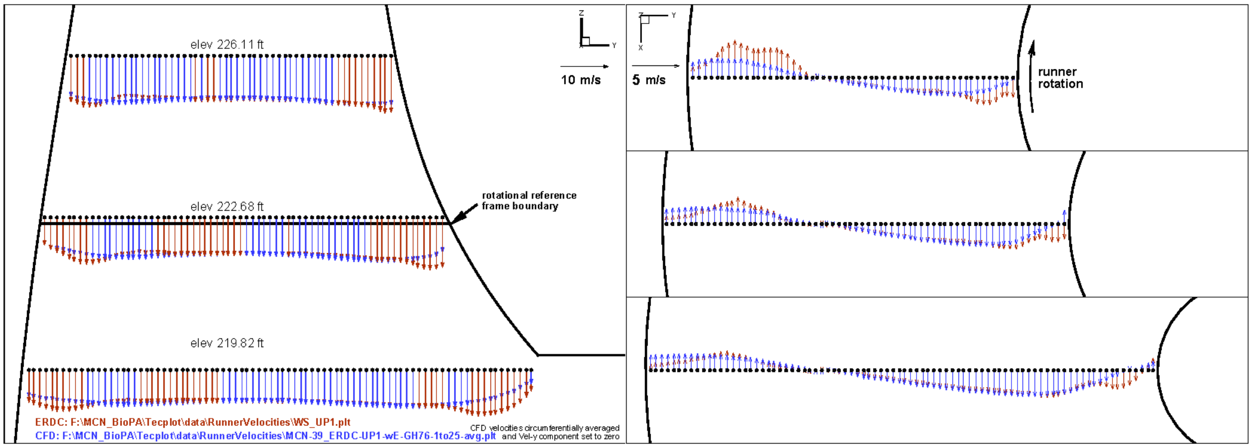

Figure D.6. Under-runner velocity comparisons for ERDC-UP1-wE-GH76-1to25.

Pacific Northwest National Laboratory

902 Battelle Boulevard
P.O. Box 999
Richland, WA 99354
1-888-375-PNNL (7665)

www.pnnl.gov